

1

NOvA Test Beam detector calibration

2

Technical Note

3

Robert Kralik

University of Sussex

4

September 12, 2023

5

Abstract

6

What is this about and what will I describe in here

7

Contents

8	1	Introduction	2
9	2	Overview of the Test Beam detector	4
10	3	NOvA calibration process	7
11	3.1	Relative calibration	12
12	3.2	Absolute calibration	13
13	3.3	Calibration uncertainties	15
14	4	NOvA Test Beam detector calibration	17
15	4.1	Overview	17
16	4.1.1	Definitions	17
17	4.2	Fiber Brightness	17
18	4.3	Simulation	17
19	4.4	Threshold and shielding corrections	18
20	4.5	Period 1	18
21	4.6	Period 2	18
22	4.6.1	Relative calibration results	19
23	4.7	Period 3	19
24	4.7.1	Relative calibration results	19
25	4.8	Period 4	19
26	4.8.1	Relative calibration results	19
27	4.9	Absolute calibration results	19
28	4.10	Drift in TB data	25
29	4.11	Results	25
30	4.12	Validation	25

31 1 Introduction

32 TO DO:

- 33 • Divide the motivation to abstract (why do we care about test beam calibration, what did
34 we do and how did we do it. What are the results)
- 35 • and introduction (brief history of test beam calibration, maybe a bit more detail into why
36 is test beam calibration important)

37 Why is Test Beam? "The idea, as with any test beam experiment, is to expose a detector
38 to a beam of very well-characterized particles, so that we can improve our understanding our
39 how the detector responds to such particles. We make use of upstream detectors to collect
40 data on the beam particles before they interact in the NOvA detector. For example, we will
41 be able to see what a 1 GeV proton actually looks like in our detector, without having to
42 simulate it, and we can test how well we would have reconstructed the energy using our existing
43 techniques. We may find we are able to make improvements to our tools to better match what
44 we see in the detector with how we reconstruct it. Or we may find we already do a pretty
45 good job. Either way, with a full cross-comparison like this, we can be more confident in our
46 analysis of the data and reduce the level of uncertainty we consider are associated with the
47 relevant measured quantities. Ultimately, the aim will be to reduce the level of uncertainty on
48 the neutrino oscillation analyses and to make even better, more accurate measurements of the
49 Standard Model."Why is Test Beam calibration done:

- 50 • To be able to directly compare TB to the standard detectors
- 51 • To be able to verify our calibration procedures using TB data
- 52 • To study the particle response as a function of energy
- 53 • To determine an energy resolution
- 54 • To compare currently used energy scales to data and understand if we can use TB data
55 for absolute energy scale in all NOvA detectors

56 For DeltaM2: By increasing exposure, total syst. error decreases by (+) 18.5For sin2Th23:
57 Difference by reducing calib syst.: (+) 10.8Statement: "The NOvA Test Beam will improve
58 the total systema6c error on the final measurement of the oscillation parameters Dm232 and
59 sin2Th23 by 10Potential Test Beam impacts: Check modeling of hadronic interactions in de-
60 tector (check GEANT systemaOcs), Using Test Beam data as "single-particle MC" to train
61 CVN prong-like algorithms, Generative Adversarial Networks for MC improvements using
62 Test Beam data, Check ND calibraOon procedure to try and understand causes of 3-5

- 63 • Hadronic response and comparison with MC modeling
 - 64 – response as a function of energy
 - 65 – establishing of an absolute energy scale
 - 66 – determination of energy resolution
 - 67 – studies of topological features and resolution

- 68 * pion tracking and showers
69 * proton tracking and showers
70 – studies of timing features and resolution
71 • Electromagnetic response and comparison with MC modeling
72 – response as a function of energy
73 – establishing of an absolute energy scale
74 – determination of energy resolution
75 – studies of topological features and resolution
76 * electron signatures
77 * gamma signatures
78 – studies of timing features and resolution
79 – studies of π^0 from π^- charge-exchange
80 • Muon response and comparison with MC modeling
81 – comparison with detailed optical simulations
82 – determination of energy resolution
83 – studies of topological features and resolution
84 – cross-talk studies
85 – comparison to cosmic ray muons (requires a special trigger)
86 – studies of the muon calibration protocol
87 • Light yield and response studies as a function of particle type and detector configuration
88 – understanding the Cherenkov light contribution
89 – vertical and horizontal responses and comparison with simulations
90 – data with selected planes rotated by 45 and 90 degrees
91 – slanted (angle) plane response (and subset of programs as above)
92 – fiber attenuation studies
93 – Birks' constant studies
94 • Near / Far readout comparison
95 • Gather large libraries of particles at known energies and multiple angles of incidence to
96 help develop a CNN prong ID. Also allows training of a particle-based CVN-like PID.

97 Also use information from:

- 98 • NOvA Test Beam Technical Statement of Work
99 • NOvA Test Beam program (paper for DOE) [docdb:25074]

- 100 • NOvA Test Beam task force report [docdb:15750]
 101 • Overview presentation of NOvA Test Beam [docdb:20495]
 102 • Test Beam support document [docdb:22172]
 103 • NOvA Test Beam program proceedings [docdb:55808]
 104 Mike's proceedings from ICHEP 2020 [1].

105 2 Overview of the Test Beam detector

106 The NOvA Test Beam detector is a scaled down version of the Near and Far Detectors shown
 107 on figure 1. It is placed in the MC7b enclosure of the Fermilab Test Beam Facility in the path
 108 of the MCcenter beamline with a variety of beamline detectors to measure and identify a range
 109 of particles with various momenta [2].

110 Maybe also mention the specific times Test Beam detector was operational.

111 Majority of the Test Beam detector and it's instrumentation is identical to the other NOvA
 112 detectors, but there are a few differences, including size, scintillator oil used, readout electron-
 113 ics, or environmental controls, that we're discussing in this section.

114 Should I aslo talk about the beam halo? Could that have an influence on the calibration?

115 Maybe it's the peaks in the cosz distribution?

116 General parameters

117 The NOvA Test Beam detector consists of two 31-plane blocks, each beginning and ending
 118 with a vertical plane, with an additional horizontal plane glued inbetween them to preserve the
 119 alternating arrangement [3]. Each plane consists of 2 modules side-by-side and each module is
 120 made up of 32 cells. Each cell has an inner (without the PVC) depth and width of 5.9 cm and
 121 3.8 cm respectively, same as for the other NOvA detectors, and a length of 2.6 m. This brings
 122 the final dimensions of the Test Beam detector to 63 planes \times 64 cells, or $2.6 \times 2.6 \times 4.1 \text{ m}^3$.

123 The 63 planes are numbered from 0 to 62, with even numbers corresponding to vertical
 124 planes and odd numbers to horizontal planes. Cells are numbered 0 to 63, going from bottom
 125 to top for horizontal planes and left to right, when facing the front of the detector, for vertical
 126 planes.

127 The detector coordinate system is illustrated on figure 1. It is centered with $(0, 0, 0)$ in the
 128 centre of the first plane [4]. The x axis runs left to right when facing the front of the detector,
 129 y axis bottom to top, and z axis goes along the beam direction from front to the back of the
 130 detector. The exact geometry of the Test Beam detector from several alignment surveys is saved
 131 in gdml files and used in our analyses [5].

132 In the past we encountered an issue when aligning the Test Beam detector with the beamline
 133 measurements broke several assumptions within the Test Beam geometry [4], which manifested
 134 as uncalibrated cells in the back of the detector [6]. This was fixed by realigning both the
 135 detector and the beamline based on the last alignment survey and implemented in the production
 136 tag R23-04-05-testbeam-production.a and there after [4].

137 Should I define w here? And tehn mention it in the readout section to say that readout is
 138 always on the positive side of the detector. Additionally we use the coordinates measured by

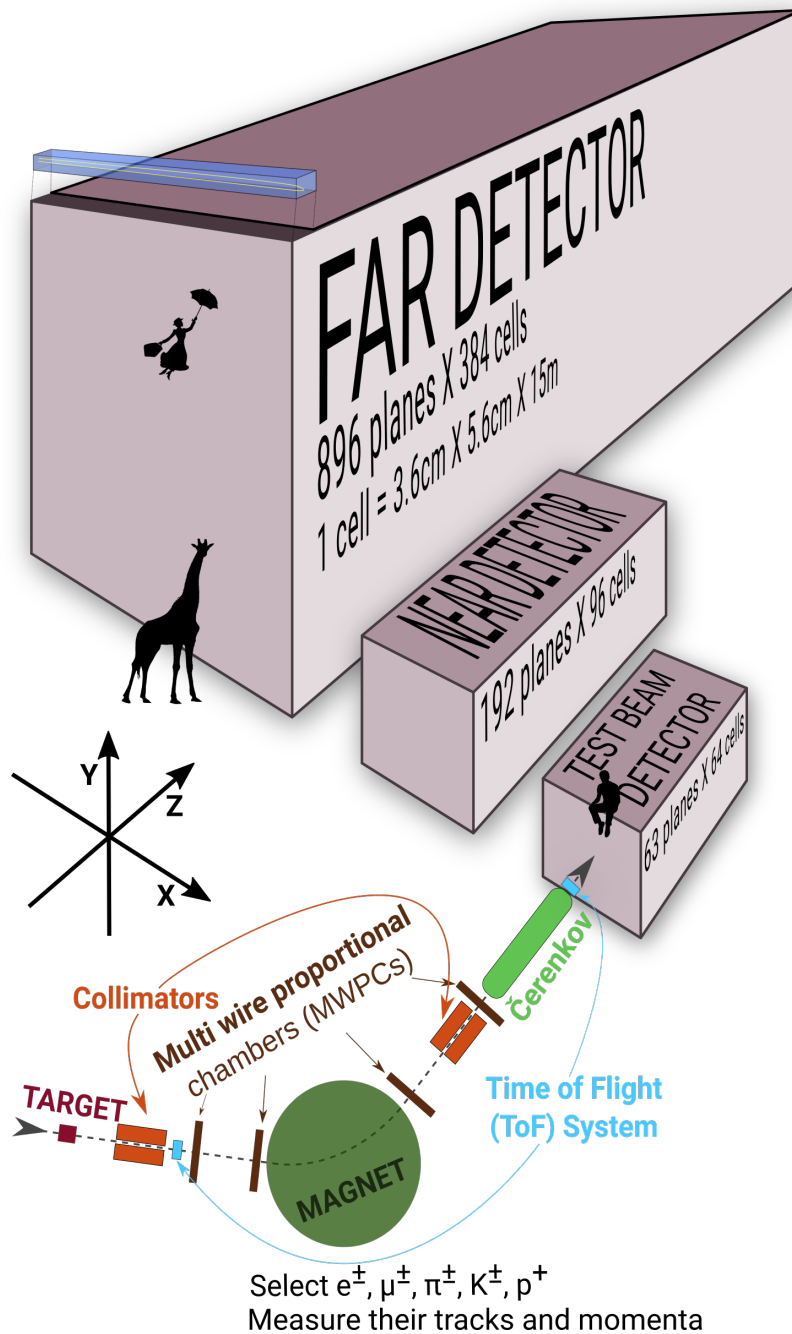


Figure 1: Comparison of Test Beam detector scale to the Near and Far NOvA detectors (and a man, giraffe, or Mary Poppins). Also shown are the Test Beam beamline detectors and components (not to scale), with arrows showing the direction of the beam. The three black arrows show the orientation fo the detector coordinate system.

- ¹³⁹ cell number V and the distance along the cell length W independent of the view in question.
- ¹⁴⁰ Extensive use of W is made throughout this document and the code. Note: W is not the distance
- ¹⁴¹ to the readout, it is simply an alias for x or y, so W = 0 is at the cente of detector. It happens that
- ¹⁴² the readout and coordinate system are arranged such that more positive values of W are closer
- ¹⁴³ to the readout. [docdb:13579 - SA The Attenuation and Threshold Calibration of the NOvA

144 detector]

145 Scintillator

146 The Test Beam detector is filled with (more than) three different versions of the NOvA scin-
147 tillator, which differ mainly in the way they were stored since the filling of the near and far
148 detectors. This is illustrated on figure 2.

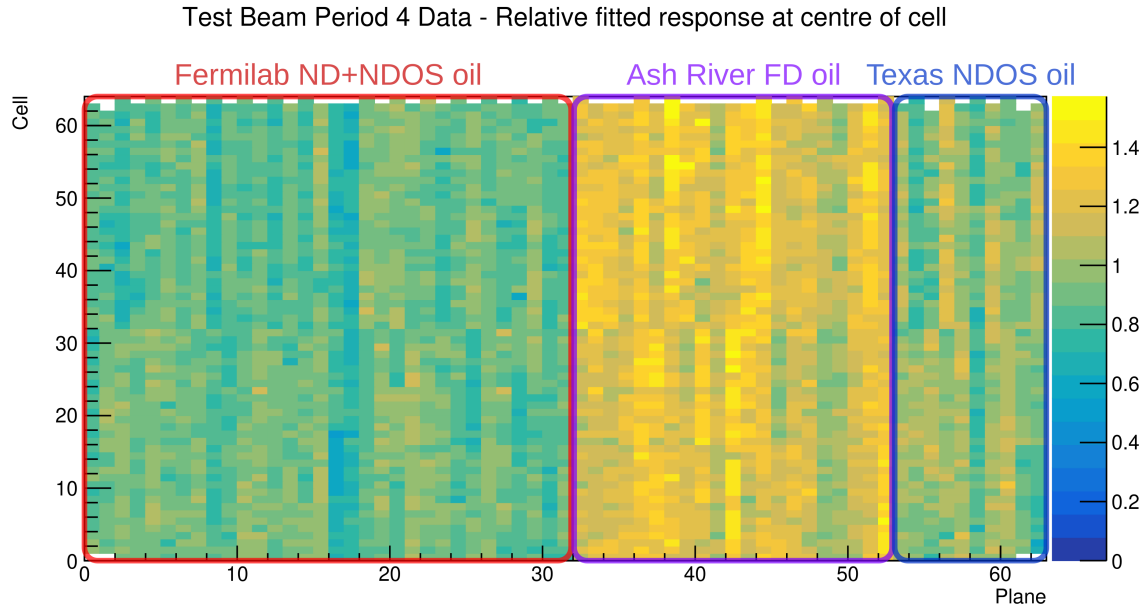


Figure 2: Uncorrected energy response in the centre of cells across the Test Beam detector showing a clear distinction between the different scintillator oils.

149 The original plan [7] was to use the scintillator from a tanker and one of the tanks located
150 outside in Fermilab. First tests showed acceptable results and the tanker oil was used to fill out
151 almost the entirety of the first block of the detector (first 32 planes) [8]. However, when we
152 loaded the oil from tank two into the tanker, it became extremely cloudy and unusable, possibly
153 due to contamination with water accumulated at the bottom of the tanks, which was mixed with
154 oil by the pump. The rest of the first block was topped up with high quality scintillator
155 from NDOS, which has been stored inside in barrels at MiniBooNE [9]. This is labeled as
156 "Fermilab ND+NDOS oil" on figure 2.

157 Even before the extreme cloudiness was discovered, it was known that the oil from the tanks
158 has lost much of its original light yield properties. Reasons vary from water contamination to
159 insects and dirt contamination [10]. Yet it was still decided to use the tank 2 oil [7]. It was
160 also decided not to mix the various oils (tanker/tank/NDOS/Ash River) as studying energy
161 deposition in different types of oils could lead to some interesting insights [10].

162 The first 21 planes of the second block (planes 32 to 52) were filled with the Far Detector
163 production scintillator shipped in from Ash River [11]. This oil has been stored in "totes"
164 inside a building and under several layers of black plastic [12]. Also used a little (70 gallons)
165 scintillator from NDOS to fill these planes (compared to 1900 gallons from Ash River) [11].

166 The last 10 planes (planes 53 to 62) [11] were filled with scintillator drained from NDOS
167 stored in Texas A&M University and University of Texas at Austin [13, 14]. This scintillator

168 has higher light yield than the one from the tanker, but lower than the Ash River one [13].

169 In total the Test Beam detector is filled with 5418 gallons of scintillator oil with a weight
170 of approximately 28.6 tons [3].

171 **Readout**

172 The Test Beam detector uses in total 126 front end boards (FEBs), each reading out signal from
173 32 cells (half of a plane) [3]. The readout is located on the top and right (looking on the front)
174 side of the detector. 118 FEBs are version 4.1, same as in the Far Detector, and 8 FEBs, located
175 on planes 16, 17, 48 and 49, are version 5.2, same as in the Near Detector. The Near Detector
176 FEBs are designed to read out data in a faster rate and we used a mix of FEB types to study the
177 difference in their response and to validate both versions in the same environment [15].

178 **Environment**

179 Unlike the near and the far detector, the Test Beam detector does not have any overburden to
180 shield it from cosmic particles.

181 Temperature very stable during winter months (heCng is installed at MC7). However, dew
182 point went over 10C ND shutdown threshold several times.

183 **Underfilled cells issue**

184 The Test Beam detector is slightly tilted around the Z axis by about 0.7° towards the readout.
185 This caused the top cells of both modules of all the horizontal planes (cells 31 and 63) to be
186 underfilled, creating an air bubble on the left side of the detector and severely affecting the
187 energy response in those cells [15]. This has been fixed [16] by adding extensions to the filling
188 ports and overfilling the horizontal cells with the NDOS scintillator stored in drums Fermilab
189 (not the scintillator store in a tanker or tanks). This scintillator was also used in the first half
190 of the detector (Fermilab ND+NDOS oil on figure 2), but is different from the "Ash River oil"
191 used in part of the second half of the detector (bright part of figure 2). The overfilling was done
192 in April 2021 in 3 stages in between the full operation of the Test Beam detector.

193 **3 NOvA calibration process**

194 Test Beam is following the same ideas and procedures as the standard NOvA calibration. This
195 section intends to provide only a brief overview of the NOvA calibration. Further details can
196 be found in the other NOvA calibration technical notes [17].

197 The purpose of calibration is to make sure that we get the same amount of energy wherever
198 or whenever it's deposited in whichever of NOvA's detectors and to express this energy in phys-
199 ical units. The NOvA calibration uses cosmic ray muons, which provide a consistent, abundant
200 and well-understood source of energy deposition and consists of two closely connected parts
201 [18]:

- 202 1. The **relative calibration** corrects for attenuation of scintillator light as it travels through
203 the cell to the readout, as well as for differences between detector cells.

204 2. This is followed by the **absolute calibration**, which only uses stopping muons when they
 205 are minimum ionising particles and calculates a scale between the measured charge read-
 206 out, corrected by the relative calibration, and the simulated energy deposition in physical
 207 units of MeV. This scale is calculated for each time period and each detector separately,
 208 which ensures the energy deposition is directly comparable wherever or whenever it oc-
 209 curred.

210 There is also **timing calibration**, which corrects for the time differences of the signal to be
 211 processed and is done as a separate project to the relative and absolute calibrations and is out
 212 of scope of this technical note [19].

213 The units and variables used to define energy deposited in NOvA detectors are listed in
 table 1:

ADC	The digitized charge collected by the APDs from the Analog to Digital Converter [20].
PE	Number of Photo Electrons. Calculated by a simple rescaling of the best estimate of the peak ADC. The PE per ADC scale only depends on the FEB type and the APD gain settings. This is technically done before the calibration and serves as the base unit for calibration.
PECorr	Corrected PE after applying the relative calibration results. The correction is a ratio between an average energy response (a pre-determined semi-arbitrary number) and the result of the the relative calibration fit (also called attenuation fit), which depends on w, cell, plane, epoch and detector. This makes the energy response equivalent across each detector.
MEU	Muon Energy Unit is the mean detector response to a stopping cosmic minimum ionising muon. Mean MeV/cm or mean PECorr/cm
MeV	Estimated energy deposited in the scintillator calculated from PECorr using the results of the absolute calibration. Additional correction for dead material needs to be made in order to get a calorimetric energy estimate.

Table 1: Definitions of variables commonly used in calibration [17, 18].

214 The final result of the NOvA calibration is the deposited energy in terms of physical units,
 which is in effect calculated as:

$$E_{dep}[\text{MeV}] = \underbrace{\frac{\text{MEU}_{truth}[\text{MeV}/\text{cm}]}{\text{MEU}_{reco}[\text{PECorr}/\text{cm}]}}_{\substack{\text{Absolute calibration} \\ (\text{Detector, epoch})}} \times \underbrace{\frac{\text{Average response}[\text{PECorr}]}{\text{Fitted response}[\text{PE}]}}_{\substack{\text{Relative calibration} \\ (\text{Detector, epoch, plane, cell, w})}} \times \underbrace{\left[\frac{\text{PE}}{\text{ADC}} \right]}_{\substack{\text{Scale} \\ (\text{APD Gain, FEB})}} \times \text{Signal}[\text{ADC}], \quad (1)$$

215 where both the relative calibration results (blue fraction) and the absolute calibration results
 216 (red fraction) are stored in a database and applied together with the ADC-to-PE scale by the
 217 NOvASoft *Calibrator* package during processing of every hit in the NOvA detectors.

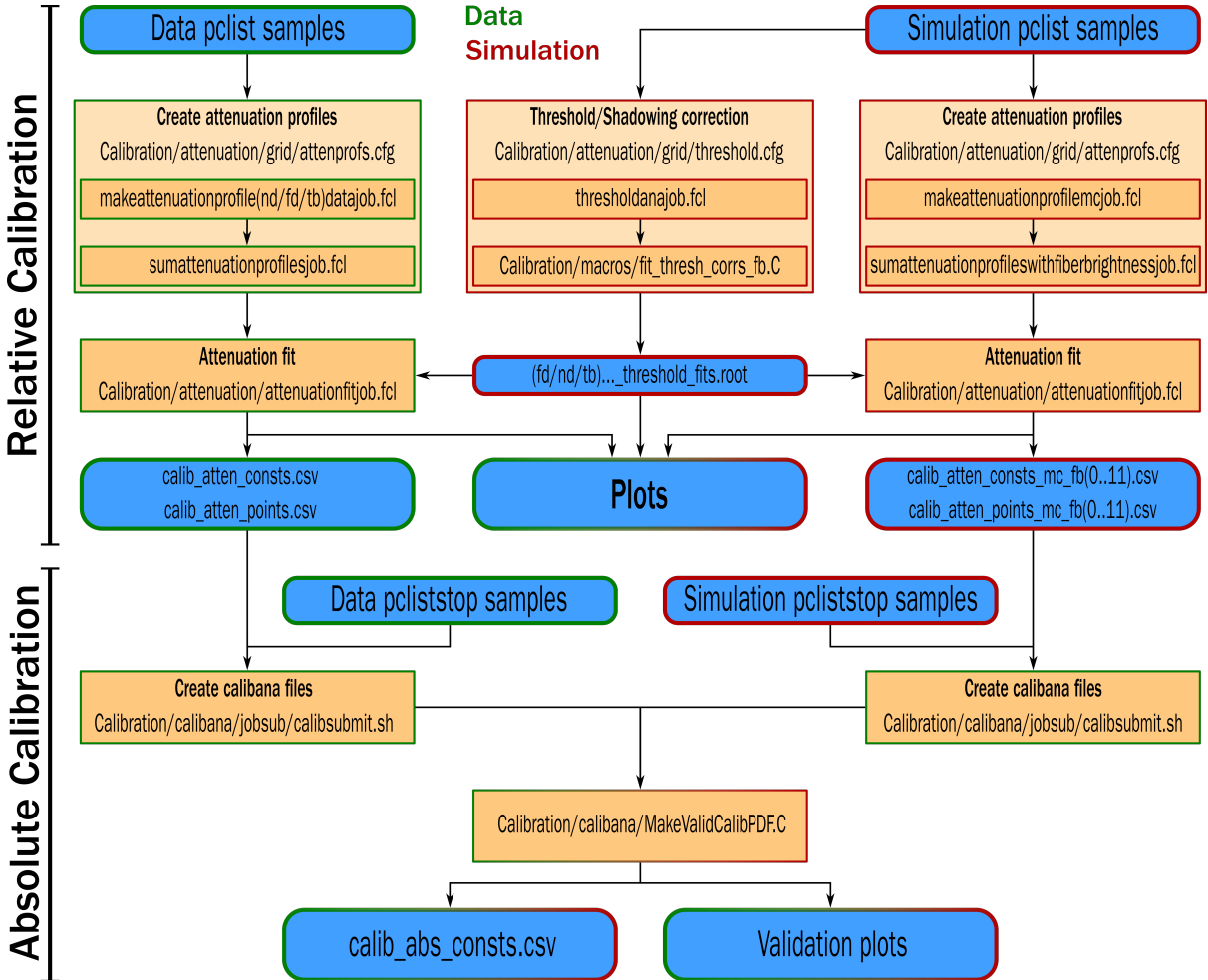


Figure 3: Flow chart showing the jobs (orange background) and files (blue background) needed and produced during the full NOvA calibration process. The left chain is showing the data calibration process (with green border) and is applied to every data calibration sample separately (periods or epochs). The center and right chains are showing the simulation calibration process (red border), which is redone only if there's a change to the detector simulation. The absolute calibration at the bottom combines data and simulation. The entire process is done separately for each NOvA detector.

218 **Creating calibration samples**

219 To select good quality cosmic ray muons we first remove beam related events based on their
 220 time stamp relative to the time of the beam spill, as shown on figure 4. Then we apply basic
 221 reconstruction and track-based selection.

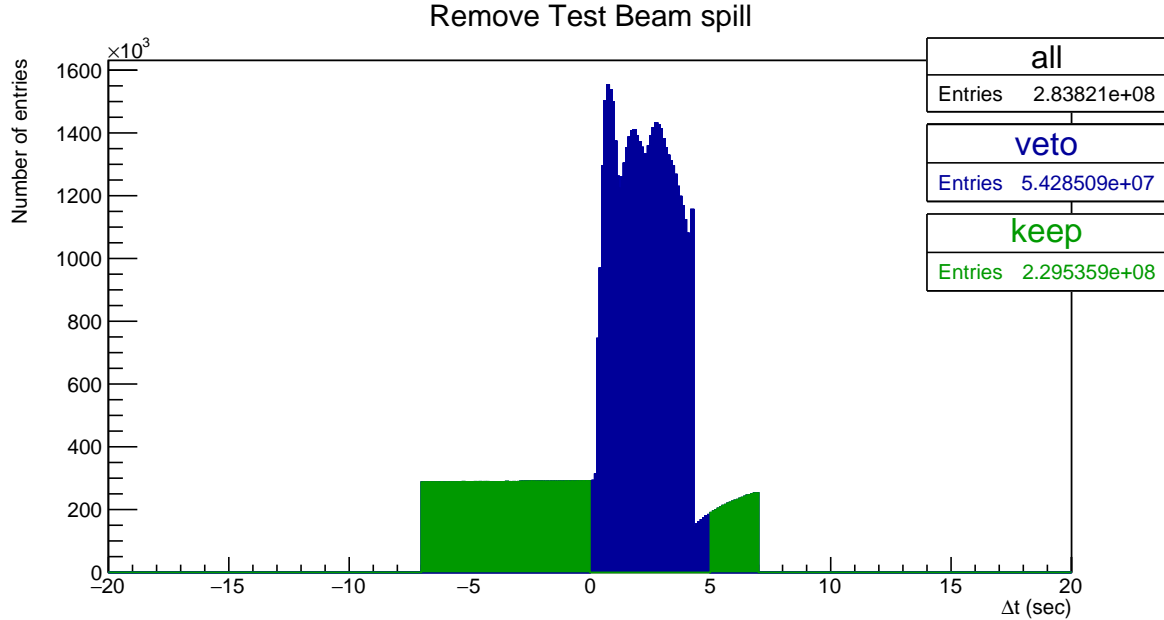


Figure 4: Test Beam beam spill events removed from the calibration samples. Test Beam beam spill is 4.2 seconds long and we remove events (in blue) within a 5 seconds window from the start of the beam spill. The remaining events (green) should mostly consist of cosmic particles. This example and the numbers of entries are for the full period 4 Test Beam sample.

222 Since energy deposition in a cell depends on the pathlength the particle traveled through
 223 the cell, we only use hits for which we can reliably calculate their pathlength. We call these
 224 hits **tricell** hits, as we require that all accepted hits also have a recorded hit in both neighboring
 225 cells of the same plane, as shown on figure 5. In case there's a bad channel in a neighboring
 226 cell, we ignore this channel and look one cell further. We can then calculate the pathlength
 227 simply as the cell width divided by the cosine of the direction angle [17, 18].

228 For the absolute calibration we select muons that stop in the detector. For this we identify
 229 muons with a Michel electron at the end of their track and only selection those [21].

230 For each data period/epoch and each simulation version we create two calibration samples
 231 that are used as the input for the relative and absolute calibration. The samples are called [22]

- 232 • pclist = **list** of **pre**-calibrated hist; Contains all selected cosmic muon events and is used
 233 in the relative calibration;
- 234 • pcliststop = pclist files only containing stopping muons used for the absolute calibration

235 **Fiber brightness**

236 For data, the relative calibration is done for each individual cell in each plane to properly
 237 account for any potential variations. Therefore we have to repeat the attenuation fit $N_{cell} \times$

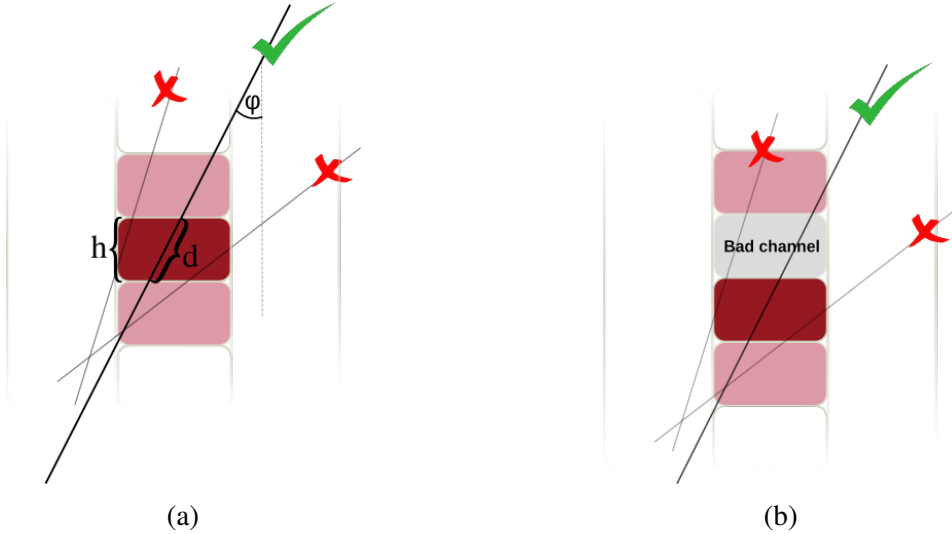


Figure 5: Illustration of the tricell condition (a). We only use hits that have two surrounding hits in the same plane to be used in the NOvA calibration. This is to ensure a good quality of the pathlength (d) reconstruction, which is calculated from the known cell height (h) and the reconstructed track angle (ϕ). In case the hit is next to a bad channel (b), we ignore this bad channel and require a hit in the next cell over.

238 N_{plane} times. However, generating enough simulated events would be very computationally
239 intensive. Additionally, we can assume that the simulated detector is approximately uniform
240 plane to plane. Therefore, for simulation, we want to *consolidate* the detector planes and only
241 consider variation in the two views and their cells, so repeat the fit $N_{cell} \times N_{view}$ times [23, 24].

242 There are some variations in the detector response cell by cell, that can be caused by differ-
243 ent fiber brightnesses, but also by different qualities of the scintillator, air bubbles, APD gains,
244 looped or zipped fibers and potentially others. To emulate these differences in the simulation
245 without the need to simulate every cell individually and properly, we divide all the cells of
246 each detector into 12 brightness bins, as shown on figure 6. These bins describe the relative
247 differences in the detector response between individual cells [24].

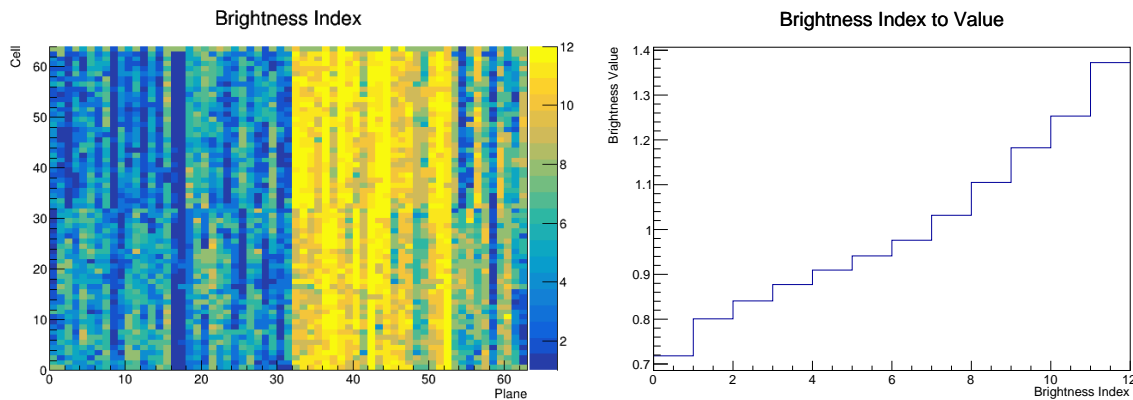


Figure 6: The Test Beam detector is (like the standard NOvA detectors) divided into 12 brightness bins (left plot), each representing a relative difference in energy response (right plot) due to different brightnesses of the fibers, scintillators, or readout.

248 **Threshold and shielding correction**

249 Energy deposited far away from the readout may get attenuated enough to be shifted below
250 the threshold. These low energy depositions would be missing from the attenuation fit, biasing
251 it towards larger light levels going away from the readout. A similar effect, specifically for
252 the vertical cells, is caused by using cosmic muons for calibration. The top of the detector ef-
253 fectively shields the bottom of the detector, skewing the energy distribution of cosmic muons.
254 To correct for both of these effects, we use simulation to calculate the threshold and shield-
255 ing (also called threshold and shadowing) correction by comparing the true and reconstructed
256 information. We apply this correction before the attenuation fits [23].

257 **3.1 Relative calibration**

258 Detailed description can be found in the "Instructions for the Attenuation Calibration Job"
259 technote from Prabhjot from docdb:13579 (list of all calibration technotes) and on the relative
260 calibration wiki page.

261 Relative calibration/attenuation correction (the exact commands are shown on figure 3).
262 This is taken from / inspired by Prabhjot technote. Maybe here I can just refer to the flowchart
263 for the commands but for TB I can specify what are the commands exactly. Maybe write down
264 a simple cook book for TB calibration.

- 265 1. Create the threshold/shadowing corrections
- 266 2. Create attenuation profiles, which are profile histograms of PE per pathlength as a func-
267 tion of w through each cell for all planes.
- 268 3. Analyse the calibhist files and draw the histograms
- 269 4. Apply the threshold and shielding correction
- 270 5. Do the attenuation fit, which consists of
 - 271 (a) exponential fit for both the short and the long path
 - 272 (b) LOWESS

273 Create attenuation profiles. Attenuation profiles have a constant binning $fNBins=100$ (in
274 w), same for ND, FD and TB. This results in an effectively finer binning for TB compared
275 to ND and FD. For FD $w = (-900, +900)$, ND: $(-250, +250)$, TB: $(-150, +150)$. TB: 3cm/bin,
276 ND: 5cm/bin, FD: 18cm/bin. What effect could this have on the relative calibration results?
277 Particularly on the calibration shape?

278 Do the fit. What exact fits are we using and in what order? Exponential, fit to residuals...

The attenuation fit considers both short- and long-path light (i.e. when a photon goes straight to the readout and when it loops around the cell first). The profile in a channel is fit to the form,

$$y = C + A \left(\exp\left(\frac{W}{X}\right) + \exp\left(-\frac{L+W}{X}\right) \right), \quad (2)$$

279 where y is the response, L is the cell length, C and X are the free parameters in the fit. X
280 gives the attenuation length as well. Initially, the fit is to the central part of the cell, which

281 is different for each detector. In addition to the approximately quartic behavior at the ends of
 282 every channel there are in many channels fairly large residuals. They don't appear to follow
 283 any consistent pattern. The leading hypothesis is that these are due to varying fiber position
 284 within the cell. Usually the fiber lies in the corners of the cell, but if it is somehow twisted so
 285 that it rises into the center of the cell, then it should collect more light, to an extent comparable
 286 to what is seen here. To remove such an irregular pattern, the residual from the analytic fit
 287 is simply fit with LOcally WEighted Scatter plot Smoothing, LOWESS. The LOWESS curve
 288 at each point is formed from the weighted mean of the deviations. The weighting function is
 289 the traditional tri-cube, (insert equation, likely not needed for this technote) [docdb:13579 -
 290 SA The Attenuation and Threshold Calibration of the NOvA detector, already in 1stAna and
 291 Backhouse's technote]

292 For NDOS the fit was a very little bit different, where we didn't use L but $3L/2$. Also it says
 293 that "Over the length of an NDOS cell, the effect of the long attenuation length is imperceptible,
 294 and is modelled as a constant (If you put a long attenuation term in, the fit drives the length
 295 scale to infinity anyway). [docdb:7410]

In many channels, fairly large residuals are visible. They don't appear to follow any consistent pattern. The hypothesis is that these are due to varying fibre position within the cell. Usually the fibre lies in the corners of the cell, but if it is somehow twisted so that it rises into the centre of the cell, then it should collect more light, to an extent comparable to what is seen here. To remove such an irregular pattern, the residual from the analytic fit is simply fit with LOWESS (locally weighted scatterplot smoothing). The LOWESS curve at each point is formed from the weighted mean of the deviations. The weighting function is the traditional tri-cube:

$$w_i = \left(1 - \left|\frac{x - x_i}{\sigma}\right|^3\right)^3. \quad (3)$$

296 The smoothing length scale σ is 30cm. 20 points calculated by this method are stored, to be
 297 linearly interpolated between to approximate the full LOWESS curve. If the LOWESS fit at
 298 any point exceeds 15% the original attenuation fit was very bad, and the channel is marked
 299 uncalibrated. Figure 4 shows an example of large (10%) deviations being fitted. This variation
 300 is not seen in the MC, and so the LOWESS fit is skipped there. Due to the lower stats available
 301 in MC, instead of being collated by plane and cell, the curves are only calculated by view and
 302 cell. [docdb:7410]

303 The current value of σ in the code is $1.5 \times \text{DetWidth}/20$

304 Now we have the relative calibration done and the constants saves. What are the const and
 305 points files that we get? What do they mean?

306 3.2 Absolute calibration

307 Apply cuts and get an average PEcorr response for each epoch/period individually and for each
 308 view. Get an average over the two views.

309 Save the results.

310 Stopping muons provide a good sample of known energy deposits. If we can collect a
 311 "golden" sample, they should provide the scale factor to convert PEcorr to GeV. So far, the
 312 method used has been imperfect, and the absolute calibration constants are known to be off
 313 by approx. 10%. Since a factor already has to be derived to correct for dead material, this is

314 not significantly impeding current efforts, but work was recently gone into improving this area.
 315 [docdb:7410 - this was likely before the track window cut was introduced] (Here it says that it's
 316 not such a big a problem since we have to scale for the dead material anyway. But nowadays we
 317 have to account for a large systematic uncertainty in the absolute energy scale in our analyses.
 318 How is the dead material correction different from the energy scale uncertainty?)

...the calibration of the calorimetric energy scale of the NOvA detectors uses the energy deposited by stopping muons as a standard candle. To reduce systematic uncertainties, only those energy deposits in a 1-2 m window away from the muon track end point are used. The mean of the detector response distribution is found for data and MC in both near and far detectors. The mean of the distribution of true energy deposits in the track window is used to provide a conversion factor between the detector response and the true energy deposited in the scintillator for minimum ionising muons. The simulated dE/dx is uniform within about 1.8% for hits around the minimum between 100-200 cm from the track end. The energy that a muon deposits within each cell is estimated using Geant 4 and stored in Fibre Liquid Scintillator (FLS) hits. FLS hits are only those within the active material (liquid scintillator) and energy loss within the passive material (plastic extrusions) is ignored. an estimate of the minimum energy loss rate of stopping muons in the NOvA scintillator is found to be,

$$\left. \frac{dE}{dx} \right|_{\text{mip}} = (1.7915 \pm 0.0035) \text{ MeV/cm.} \quad (4)$$

319 For stopping muons in NOvA it is also important to consider their decay. The muon has a vac-
 320 uum lifetime of about 2.2 microseconds and favourably decays, with a branching ratio approx.
 321 100%, into an electron, an electron anti-neutrino and a muon neutrino. The electron produced
 322 in this decay is called a Michel electron and is used to select muons that stop within the NOvA
 323 detectors. The energy scale calibration is performed using cosmic ray muons. The calibration
 324 measures the detector response in data and MC in both near and far detectors and normalises
 325 them all by providing a conversion factor, for all four cases, that converts the detector response
 326 to energy in GeV. The energy loss rate (dE/dx) of stopping muons is well described by the
 327 Bethe-Bloch and is a function of the distance from the stopping point. A track window tech-
 328 nique is used to minimise the variations in detector response that depend on the distance to
 329 the track end. Using this technique only hits within a region of distances from the track end
 330 are used. The position of the track window is chosen such that a mis-reconstruction of the
 331 track end point has the minimum effect on the mean detector response. The track window is
 332 currently set to be in the range from 100 cm to 200 cm from the track end.[docdb:13579 -
 333 FA_Calorimetric_energy_scale]

334 In the First Analysis An adjustment was made to the value for the ND data to lower the
 335 value of PEcorr/cm by about 3.6%. The adjustment was made based on studies of muons from
 336 beam neutrinos interacting in the detector where it was observed that the average beam muon
 337 response was 3.6% lower in data than in MC [8]. For the FD There is a discrepancy in the
 338 distributions of PEcorr/cm in data and MC; the mean of the distribution is higher in data than
 339 in MC. This may be due to mis-modelling of the detector response in the MC. In any case, the
 340 data-MC PEcorr/cm discrepancy is tuned out when the calorimetric energy scale is applied.
 341 [docdb:13579 - FA_Calorimetric_energy_scale]

342 The calibration constants are written to the database tables calib atten consts and calib atten
 343 points. The calib atten consts table contains the seven free parameters in the attenuation fit, plus
 344 identifying information. The calib atten points table contains the 20 LOWESS points for each

345 cell, with one point per row. When a request comes to Calibrator to create a RecoHit, usually
346 from a RecoBase object that has provided a W value based on a straight-line extrapolation of its
347 trajectory, ultimately we end up in Calibrator::GetPECorr. This retrieves an AttenCurve object
348 from a cache we hold of all the database values, which can calculate the mean response to
349 cosmic rays at any position. The calibrated energy deposit is then the PE in the CellHit divided
350 by this average cosmic ray response. A correction factor taken from the absolute calibration,
351 also stored in the database, is applied to the answer to give the resulting PECorr. Calibrator also
352 stores the quality of the calibration fit for a given cell such that if we fail to calibrate a cell in the
353 Data to a sufficient quality that cell will not return a calibrated energy in both Data and Monte
354 Carlo. Calibrator also returns the MIP and GeV scales that are described in the accompanying
355 absolute calibration technote. [docdb:13579 - SA The Attenuation and Threshold Calibration
356 of the NOvA detector] ...The calibrated energy deposit is then the PE in the CellHit divided
357 by this average cosmic ray responseAn eyeballed factor of 75 is applied to the answer to give
358 the resulting PECorr about the same size as the input PE (this is the factor (originally) used)
359 [docdb:7410]

360 Describe that the results of the calibration process are store in csv tables and loaded during
361 processing of each event.

362 From Calibration_Meta_READFIRST.pdf: Validations of any calibration correction take
363 the same basic form:

- 364 1. What deficiency are you correcting for? (For Test Beam this would be the difference
365 between the different scintillators, also the faulty FEBs, distribution of w is not flat,
366 especially in the overfilled cells. The energy response between the different cells and
367 planes is not the same. Maybe I should talk about this for each period separately when I
368 have the calibhist plots which show the non-linearities. Also the PhotonTransport plots
369 don't really show the PECorr but the PE/cm itself but with the fit!!!
- 370 2. What correction factors/scales have you found? Show them in plot form. (This is basi-
371 cally the PhotonTransport plots for the relative calibration and the pecorrem distributions
372 for the absolute calibration)
- 373 3. Now generate the same plots as in (1) but with the corrections applied. Technically this
374 is the absolute calibration validation plots. Does this mean that the PE/cm plots from the
375 absolute calibration should be/are exactly the same as the calibhist plots? Not entirely
376 as those are only for the stopping muons, whereas the calibhist are for the through-going
377 muons. Does it mean I should maybe generate the calibhist plots with the relative cali-
378 bration applied?
- 379 4. Ratios of plots in (3) to (1) to highlight any patterns or difficult-to-spot discrepancies
380 between what we think should happen when the constants are applied, and what does
381 happen. But what does this tell us? It's basically just an average of the attenuation
382 correction...

383 3.3 Calibration uncertainties

384 First Analysis systematic uncertainties due to calibration: Sources of systematic uncertainty
385 of particular concern are those introduced by residual variations remaining after calibration.

386 Systematic errors are introduced by spatial and temporal variations in detector response. Fur-
387 ther, any difference between the two detectors may introduce a relative shift in the energy
388 scale between the detectors. A source of systematic uncertainty can be introduced by mis-
389 reconstructing the end point of the muon track. Such a mis-reconstruction would shift the
390 window within which hits are selected and hence the dE/dx of the muon. The figure shows
391 that the detector response varies by up to about 60% over the range from 0 to 500 cm to the
392 track end. This large variation illustrates the importance of careful consideration of the track
393 window position and size. The detector response for both data and MC is minimum at about
394 130 cm from the track end and is flat to about 1% in the range from 100 cm to 200 cm from
395 the track end. For a track window starting at 100 cm from the track end, a conservative mis-
396 reconstruction of the track end point by 10cm will shift the start of the track window to between
397 90cm and 110cm. This shift will alter the MEU value by less than 0.4% over the range. If the
398 calibration procedure was ideal the detector response would not vary with position in either
399 data or MC. The calibration is not ideal and the detector response and recorded simulated en-
400 ergy deposition varies with position of the hit within the detector, such variations will introduce
401 systematic errors. The position of a hit can be defined by the plane, cell within the plane, and
402 distance along the cell (w) of the hit. The variation in detector response and simulated energy
403 deposition vs. plane, cell and w for each view has been studied to quantify the systematic un-
404 certainty introduced by these sources. The rise in detector response at the far end of FD y-view
405 cells is an issue with several potential sources. The rise in response may be due to an accep-
406 tance effect or a light-level threshold effect among other possibilities. An acceptance effect is
407 where greater energy must be deposited at the far end of the cells so that the light can travel
408 along the fibre, hit the APD and be recorded as a hit. Both an acceptance effect and a light-level
409 effect would introduce a bias towards higher energy hits toward the far end of cells. Another
410 source of systematic uncertainty is introduced by the variation in detector response with time.
411 The FD response is stable to about 1% during the period from October 2014 to March 2015.
412 The ND response needs further study but there was no significant trend over 6 months at 5%.
413 As mentioned in Section 5, the version (7.1) of the calibration used for first analysis has been
414 adjusted based on studies of muons from beam neutrinos interacting in the detector [8]. A shift
415 of 3.6% was introduced based on the average response of muons where large sections of the
416 track were used. When only a track window of 100-200cm is used on the beam muons the
417 difference is only 2.7% [8]. Our best hypothesis for this residual 2.7% difference is that it is
418 caused by showery events that are present in ND data but not ND MC: it was shown in [9]
419 that doing the calorimetric energy scale calibration using a truncated mean (or a median or a
420 fit to the peak) gave a data/MC ratio that differed by 2.7% compared to using the untruncated
421 mean as described in this document. A comparison of various cross checks of the calorimetric
422 energy scale was undertaken (in [10] and [11]) and concluded that the nearly 5% difference
423 between ND data and MC seen in a sample of Michele electrons [12] should be applied as
424 both an absolute and relative shift to the calorimetric energy scale. The difference between the
425 level of calorimetric energy resolution of stopping muons was studied and it was found that
426 data and MC agreed best when an 8% additional smearing was introduced. Studies for the
427 NuMu analysis indicated that this was a negligible systematic uncertainty [13]. [docdb:13579
428 - FA_Calorimetric_energy_scale]

429 **4 NOvA Test Beam detector calibration**

430 **4.1 Overview**

431 History of TB calibration. What led to the final version of TB calibration. What can be done
432 next. I think this could also be in the introduction?

433 Dates and times when the data taking occurred.

434 Adding the underfilled cells to the bad channels which are automatically skipped for the
435 tricell condition

436 Period naming, possibly epochs (for P3). List of data samples, plus MC samples that were
437 used and pointer to the data-based simulation technote.

438 Specific running conditions: - maybe enough to mention this in the individual descriptions
439 of the test beam periods Underfilled cells Faulty FEBs (Period 2 and Period 3)

440 Why do we do the calibration generally and why do we need to do it for Test Beam specific-
441 ally - probably in the introduction

442 Temperature study (small overview)

443 From Teresa's thesis Along with setting the energy scale of the detector, we need to calibrate
444 the timing of the readout system for the detector. The Data Concentrator Modules (DCMs)
445 responsible for collating the data from multiple FEBs get their timing information via a daisy
446 chain originating at the detector TDU. Each DCM in the chain has a timing offset relative to the
447 DCM before it, with the last DCM having the earliest ti. Following the procedure described in
448 [66], I used timing information from hits on cosmic ray muon tracks that pass through multiple
449 DCMs to determine the relative offsets between DCMs, shown in Figure 3.20.

450 **4.1.1 Definitions**

451 List all final data and simulation definitions used.

452 Mention exactly the name and the location of the fcl files to create the TB plist/pcliststop
453 files. (Or should I only do this in the next section when mentioning the TB calibration? - yes)

454 From Teresa's thesis: "For Test Beam, we have three beam-based triggers, one pulsed trig-
455 ger, and two data-driven triggers. The data-driven triggers are both activity-based triggers. The
456 first is intended to record cosmic ray induced events for use in calibrating the detector.

457 **4.2 Fiber Brightness**

458 To divide the Test Beam detector into fiber brightness bins we used the attenuation fit results
459 for period 4 data (described in section 4.8).

460 Describe and show plots that since we are only using the fitted response at cell centre we
461 can allow fits with $\chi^2 > 0.2$. Show examples of responses with chisq larger than that and say
462 what is the final chisq chosen. No need to show the final distribution of the fb bins here as they
463 were technically shown in the general calibration description. But might refer back to it...

464 **4.3 Simulation**

465 We originally used Teresa's calibration MC sample, but after we saw disagreement, we devel-
466 oped a new MC based off of the period 3 data, which we ended up using for both period 2 and

467 period 3. For fibre brightness we are also using the same MC from period 3 data as it represents
468 the detector in its best condition.

469 We used a data-based simulation of cosmic muons for the Test Beam detector calibration.
470 The details are described in the technote XXX. We used this and this data as a basis and this
471 and this data for the fiber brightness file.

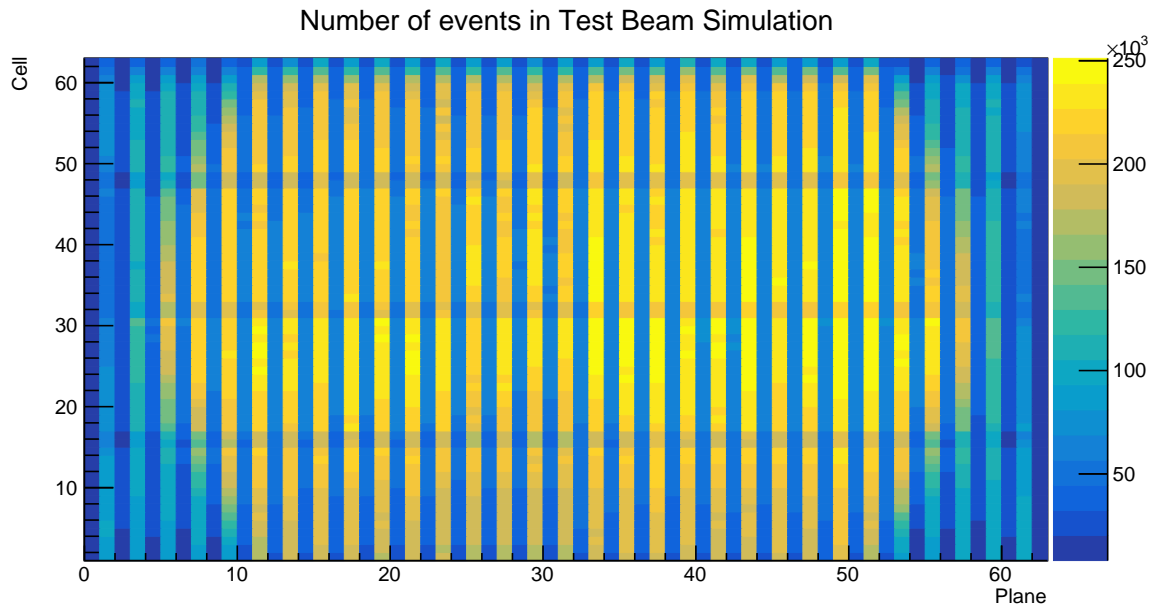


Figure 7: Distribution of events in the Test Beam simulation calibration sample.

472 **Relative calibration results**

473 **4.4 Threshold and shielding corrections**

474 The threshold and shielding correction for test beam is almost uniform across all cells as can
475 be seen on figure... This is expected as the height of the Test Beam detector of 2.6m has only a
476 negligible effect on the energy distribution of cosmic muons or on the threshold saturation. The
477 correction is basically just a normalization factor, but since the relative calibration only cares
478 about relative differences across the detector, a normalization factor doesn't change anything.

479 **4.5 Period 1**

480 Only a month of data, only first half of detector filled, primary/secondary beam halo, or over-
481 saturation leading to FEB shutoffs [docdb:38349 and 41331]. Only used for commissioning, not
482 used for any data analysis or calibration.

483 **4.6 Period 2**

484 What was done for the period 2 tb calibration, short overview of what has been done: test beam
485 data were calibrated all at the same time without splitting them to separate epochs. See figures
486 [11](#), [12](#) and [13](#).

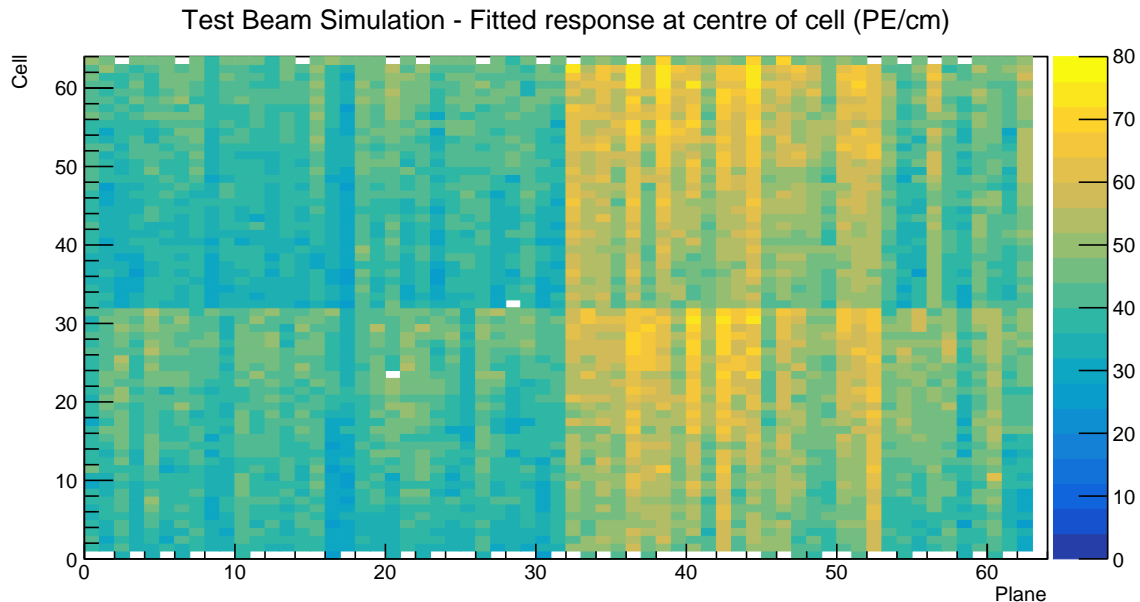


Figure 8: Overview of the relative calibration results for the Teast Beam detector simulation. Each cell represents the result fo the attenuation fit to the energy response in the centre of that cell. The blank cells are uncalibrated.

487 4.6.1 Relative calibration results

488 4.7 Period 3

489 Separation of Period 3 data into different epochs based on the running conditions (include plot
490 of the running conditions). We are separating data into pre- and post- filling states. We're using
491 only the fully-refilled post-FEB swap data from period 3 as a basis for the simulation creation.

492 4.7.1 Relative calibration results

493 Combined epochs 3a, 3b and 3c

494 Combined epochs 3d and 3e

495 4.8 Period 4

496 4.8.1 Relative calibration results

497 4.9 Absolute calibration results

498 Standard absolute calibration cuts: track window, flat-response W, positive pe, pecorr, and
499 pathlenght reco

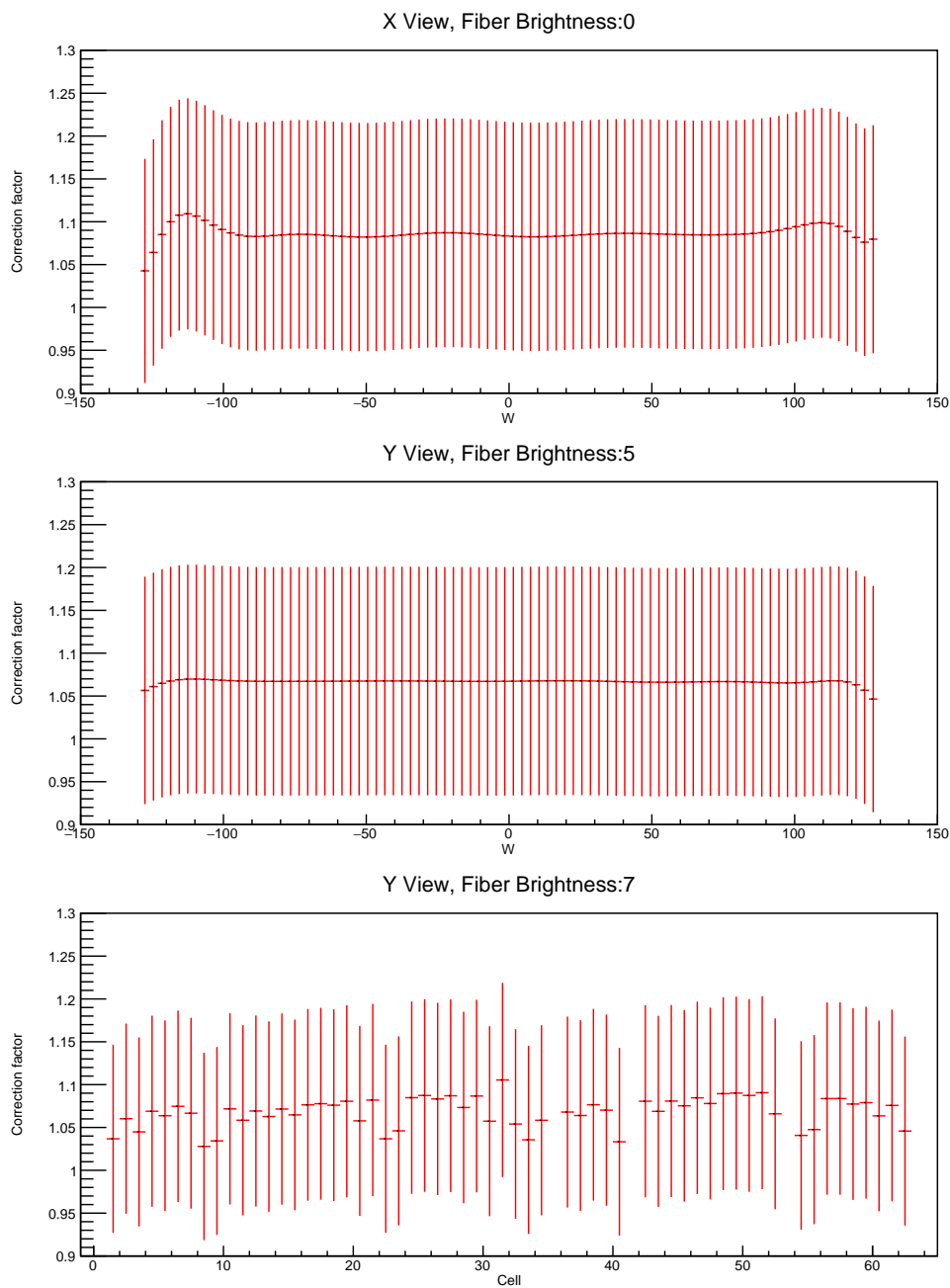


Figure 9: Examples of threshold and shielding corrections for the Test Beam detector

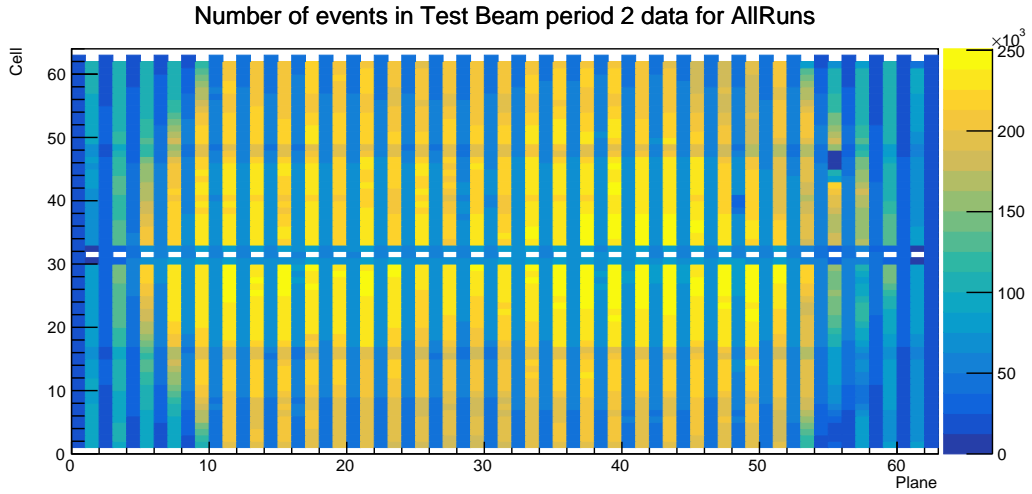


Figure 10: Distribution of events in the period 2 Test Beam data calibration sample.

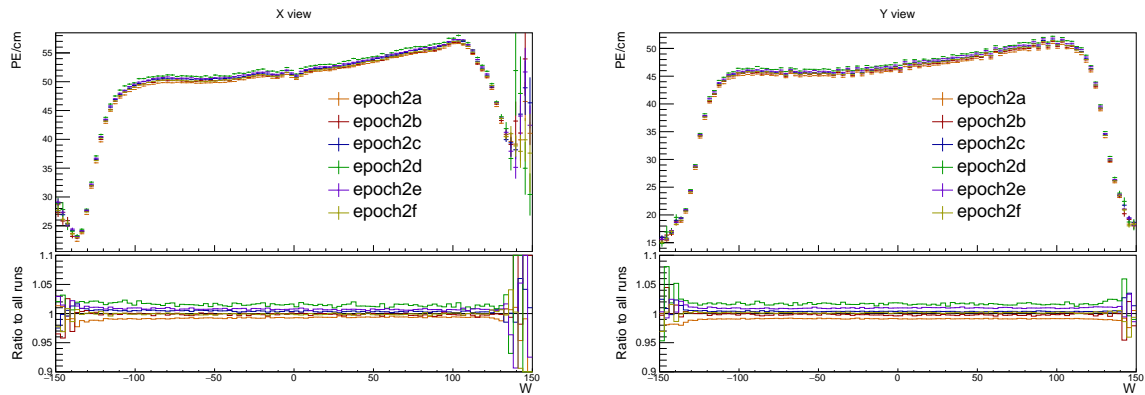


Figure 11: Uncorrected average energy response as a function of the position within a cell (w) for epochs in period 2. It is clear that there is no significant difference between the various epochs.

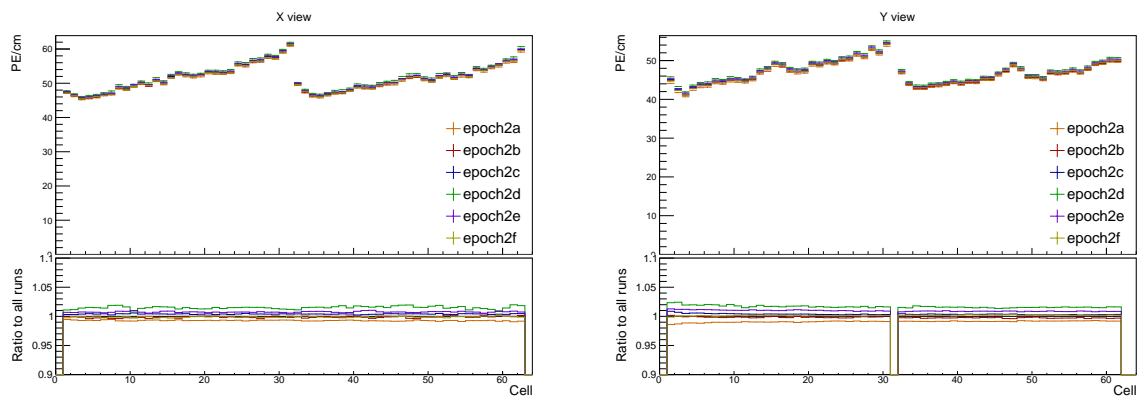


Figure 12: Uncorrected average energy response as a function of cells for epochs in period 2.

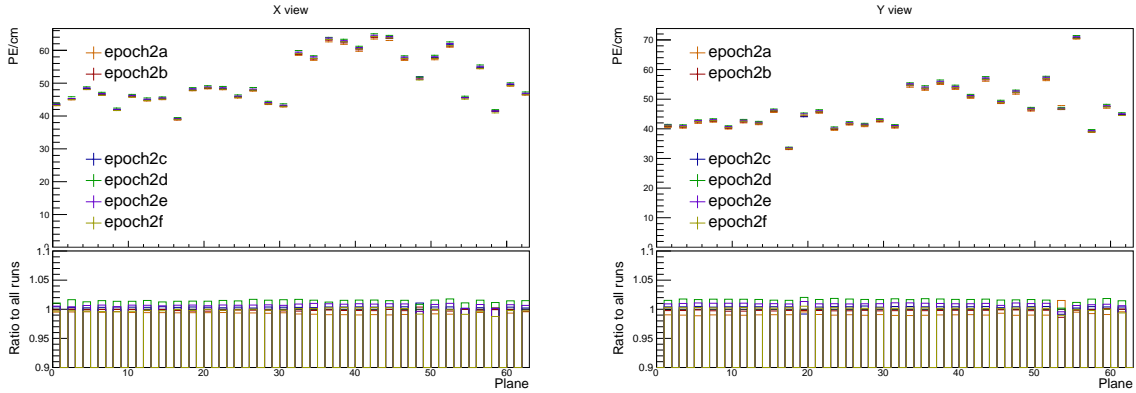


Figure 13: Uncorrected average energy response as a function of planes for epochs in period 2.

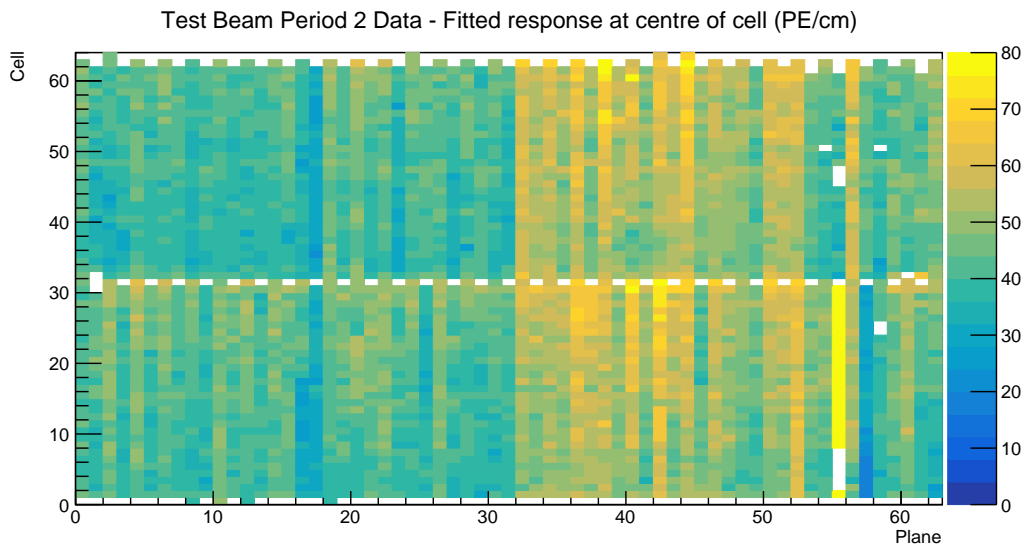


Figure 14: Overview of the relative calibration results for the Teast Beam detector period 2 data. Each cell represents the result fo the attenuation fit to the energy response in the centre of that cell. The blank cells are uncalibrated.

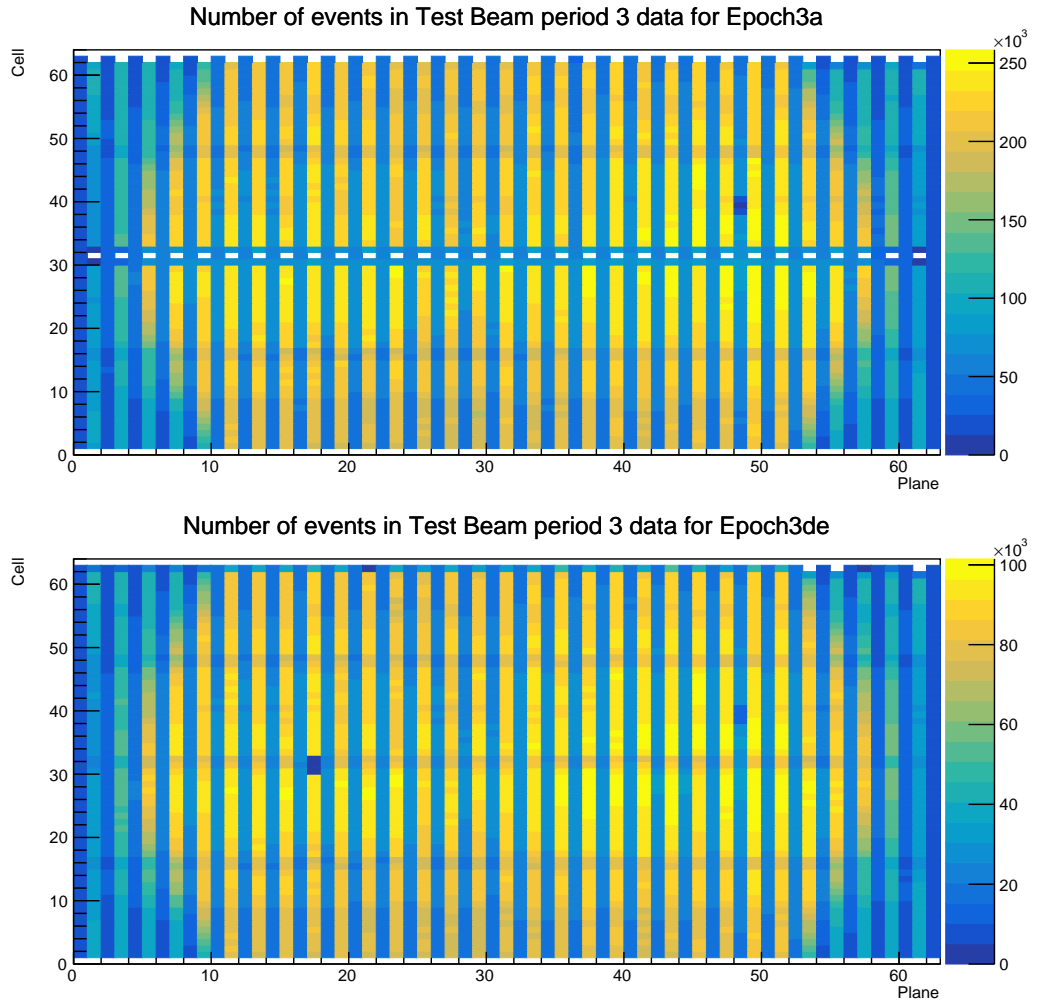


Figure 15: Distribution of events in the period 3, epoch 3a Test Beam data calibration sample.

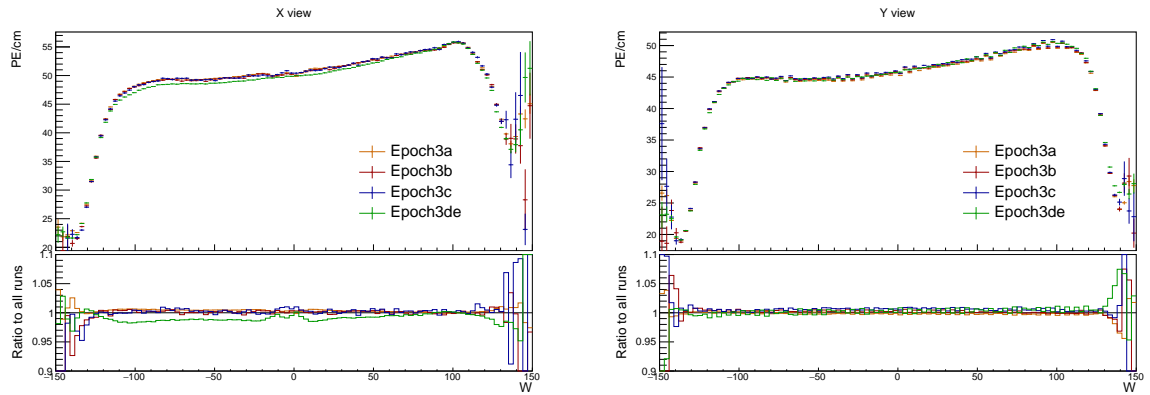


Figure 16: Uncorrected average energy response as a function of the position within a cell (w) for epochs in period 3.

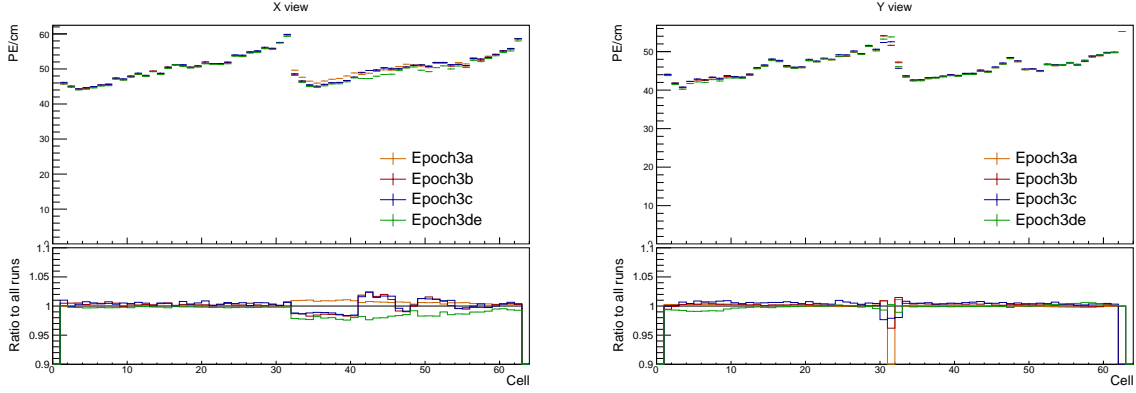


Figure 17: Uncorrected average energy response as a function of cells for epochs in period 3.

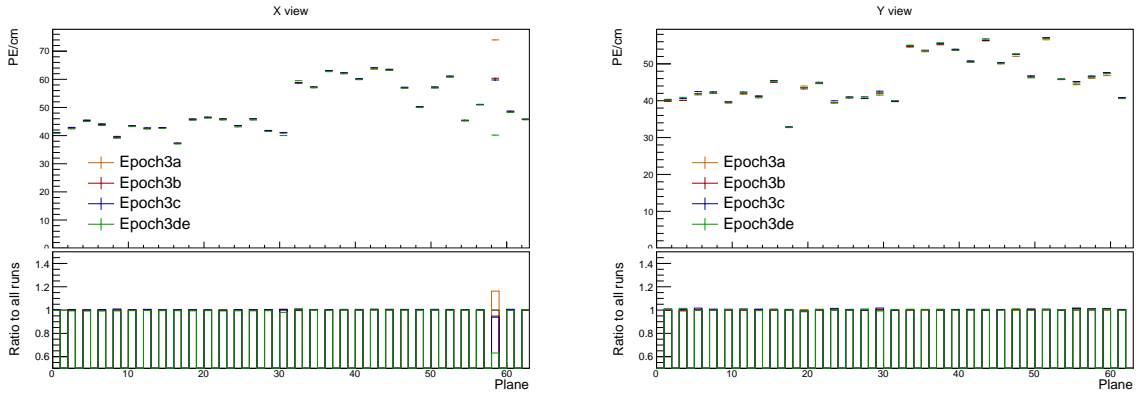


Figure 18: Uncorrected average energy response as a function of planes for epochs in period 3.

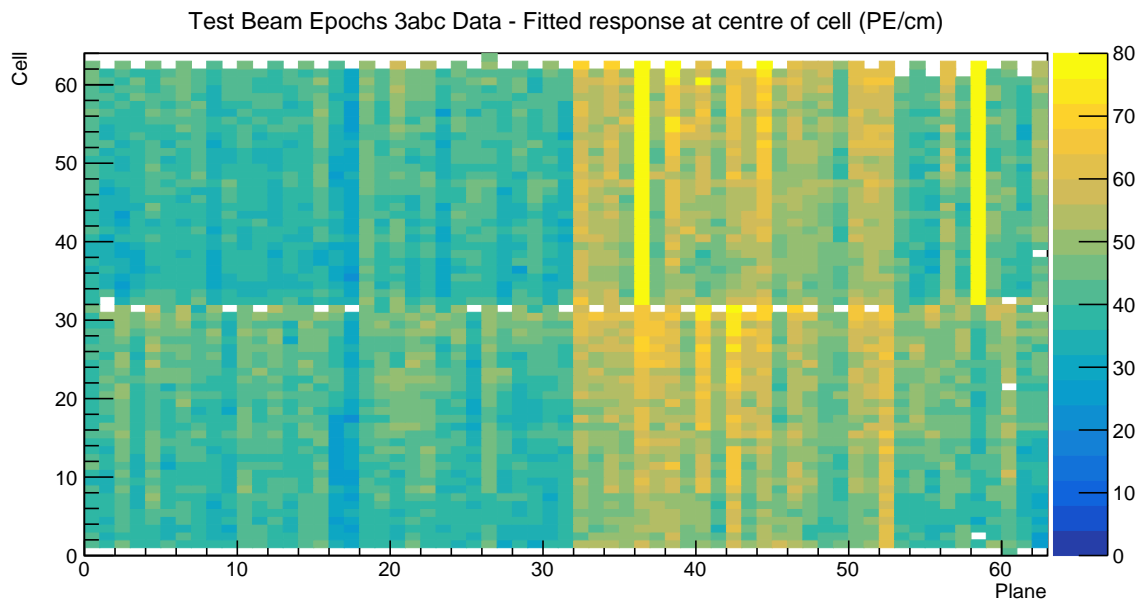


Figure 19: Overview of the relative calibration results for the Teast Beam detector period 3, combined epochs 3a, 3b and 3c data. Each cell represents the result fo the attenuation fit to the energy response in the centre of that cell. The blank cells are uncalibrated.

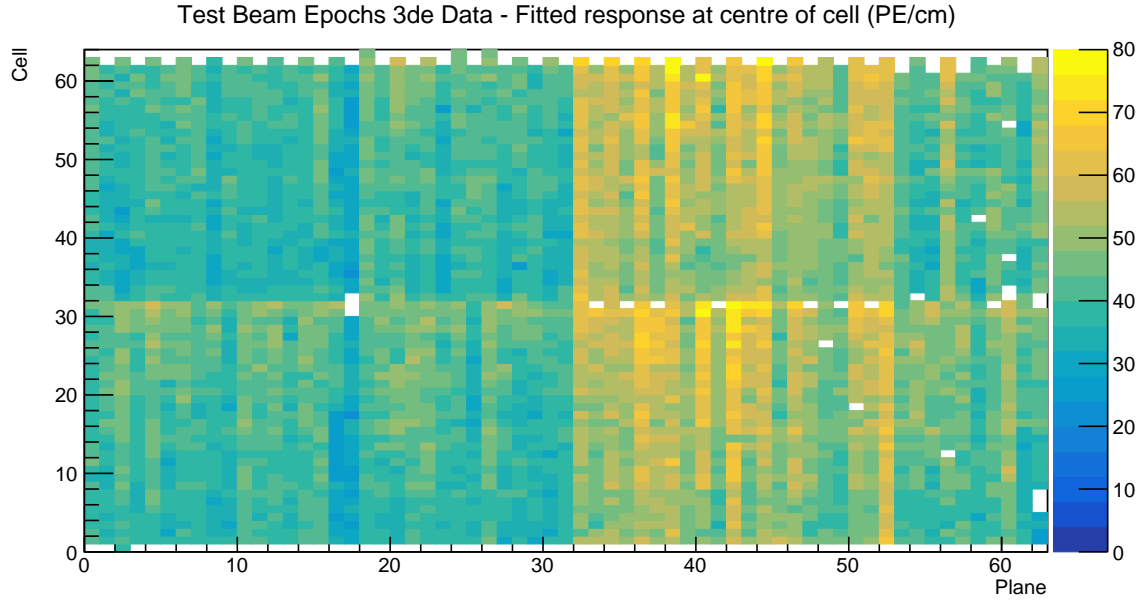


Figure 20: Overview of the relative calibration results for the Teast Beam detector period 3, combined epochs 3d and 3e data. Each cell represents the result fo the attenuation fit to the energy response in the centre of that cell. The blank cells are uncalibrated.

Sample	NHitsx	MEUx	NHitsy	MEUy	MEU	MEU Err	TrueE/dx	tE/dx Err
epoch 3abc data	2.638e+05	38.49	1.621e+06	39.4	38.94	0.006758	1.772	0.000238
epoch 3de data	1.049e+05	38.63	6.725e+05	39.42	39.02	0.01048	1.772	0.000238
period 2 data	2.322e+05	38.7	1.413e+06	39.4	39.05	0.007252	1.772	0.000238
period 4 data	5.268e+05	38.63	3.316e+06	39.4	39.01	0.004703	1.772	0.000238
simulation	2.829e+05	40.17	1.842e+06	39.93	40.05	0.006418	1.772	0.000238

501 4.10 Drift in TB data

502 4.11 Results

503 Table of final results. Final CSVs are locate in the /nova/ana/testbeam/calibration and
 504 they have been included in the vXX.XX calibration tag.

505 Plots of absolute calibration results

506 4.12 Validation

507 Comparisons with older version of calibration and maybe with the FD and ND

508 References

- 509 [1] Michael Wallbank. The NOvA Test Beam Program. *PoS*, ICHEP2020:188, 2021. doi:
 510 [10.22323/1.390.0188](https://doi.org/10.22323/1.390.0188).

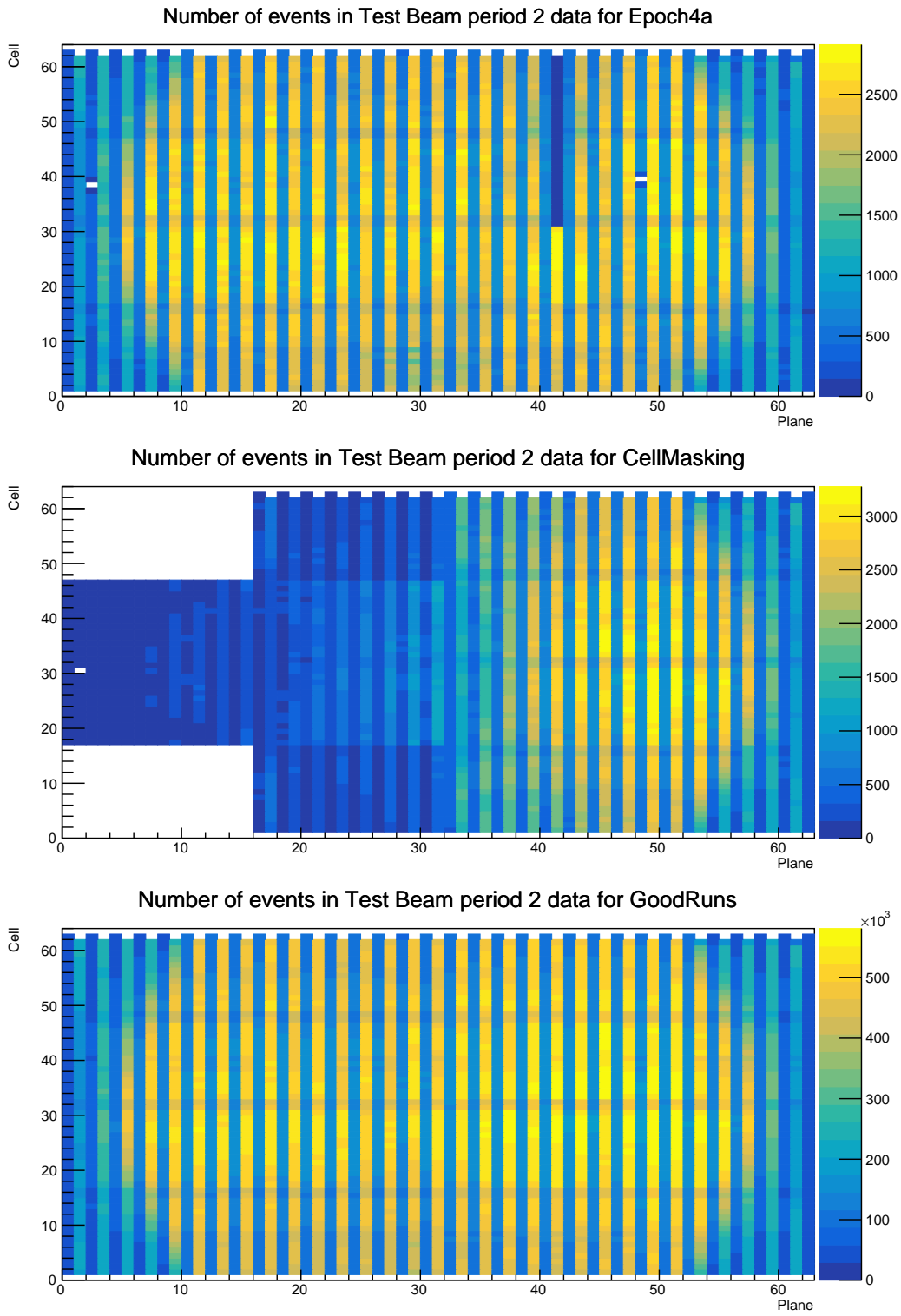


Figure 21: Distribution of events in the Test Beam period 4 data calibration sample. The top plot shows the first three commissioning runs, the middle plot the status of the detector during the Cell Masking studies and the bottom plot shows the rest.

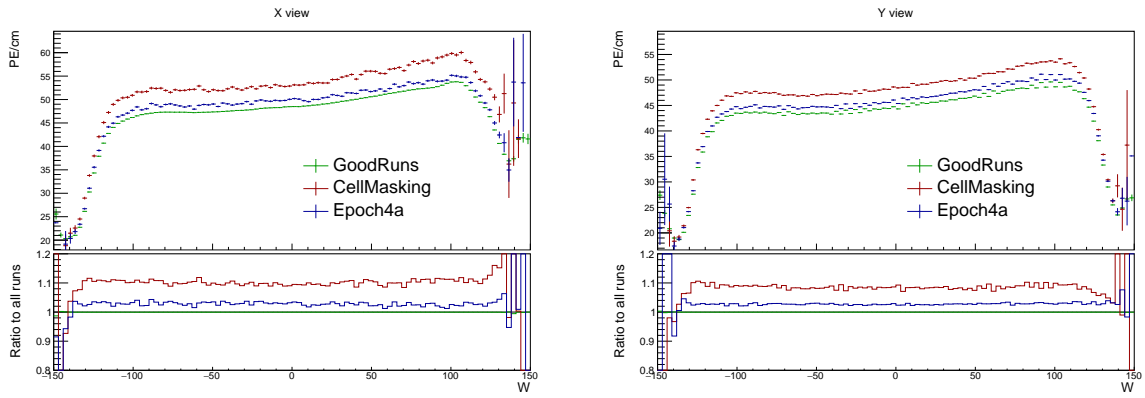


Figure 22: Uncorrected average energy response as a function of the position within a cell (w) for epochs in period 4.

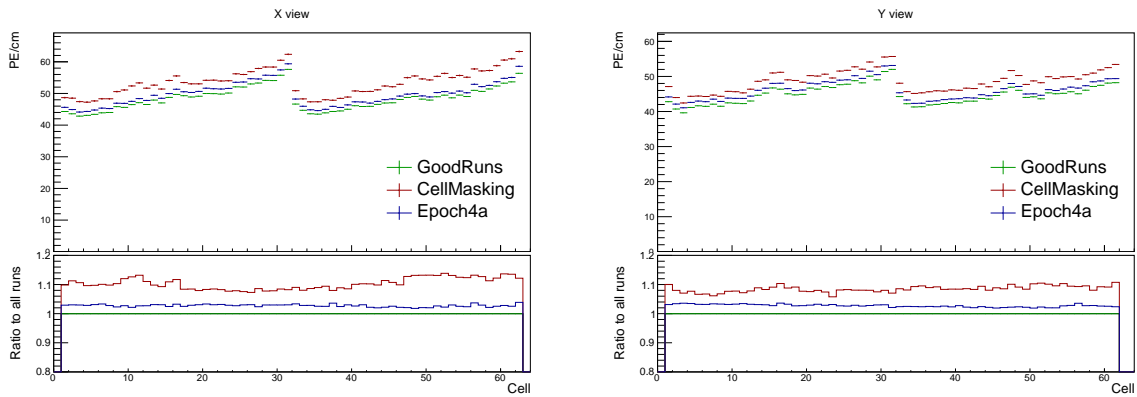


Figure 23: Uncorrected average energy response as a function of cells for epochs in period 4.

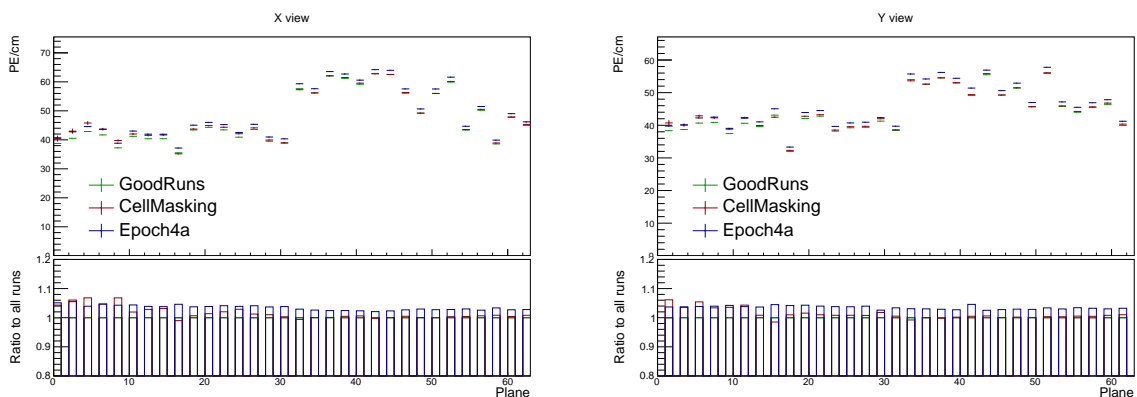


Figure 24: Uncorrected average energy response as a function of planes for epochs in period 4.

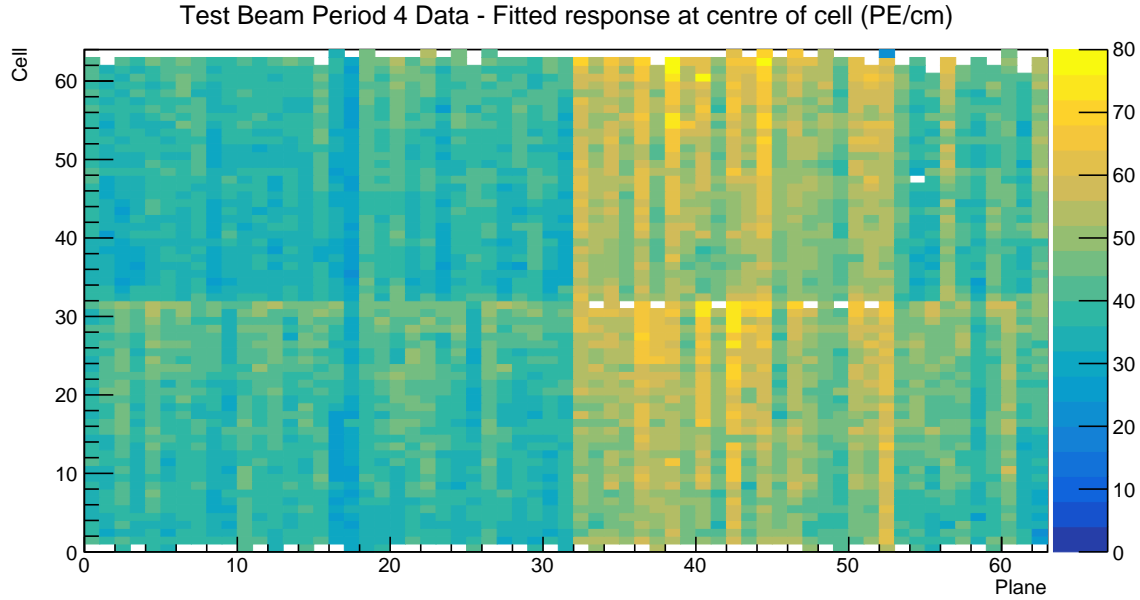


Figure 25: Overview of the relative calibration results for the Teast Beam detector period 4 data. Each cell represents the result fo the attenuation fit to the energy response in the centre of that cell. The blank cells are uncalibrated.

- 511 [2] Alex Sousa. Nova test beam status and plans - support documentation. NOVA Document
512 22172-v2, October 2017. NOvA technical note. URL: <https://nova-docdb.fnal.gov/cgi-bin/sso>ShowDocument?docid=22172>.
- 514 [3] Alex Sousa. Nova test beam plenary @ iu collaboration meeting. NOVA Document
515 29543, May 2018. NOvA internal document. URL: <https://nova-docdb.fnal.gov/cgi-bin/sso>ShowDocument?docid=29543>.
- 517 [4] Michael Wallbank. Final test beam updates (geometry and other!). NOVA Document
518 58388, April 2023. NOvA internal document. URL: <https://nova-docdb.fnal.gov/cgi-bin/sso>ShowDocument?docid=58388>.
- 520 [5] Michael Wallbank. Understanding, improving, validating the test beam geometry.
521 NOVA Document 57955, February 2023. NOvA internal document. URL: <https://nova-docdb.fnal.gov/cgi-bin/sso>ShowDocument?docid=57955>.
- 523 [6] Robert Kralik. Test beam calibration update. NOVA Document 57516-v2, January
524 2023. NOvA internal document. URL: <https://nova-docdb.fnal.gov/cgi-bin/sso>ShowDocument?docid=57516>.
- 526 [7] Alex Sousa. Test beam scintillator fill plan. NOVA Document 34196, November
527 2018. NOvA internal document. URL: <https://nova-docdb.fnal.gov/cgi-bin/sso>ShowDocument?docid=34196>.
- 529 [8] Alex Sousa. Test beam plenary update - jun. 6, 2019. NOVA Document 38349, June
530 2019. NOvA internal document. URL: <https://nova-docdb.fnal.gov/cgi-bin/sso>ShowDocument?docid=38349>.

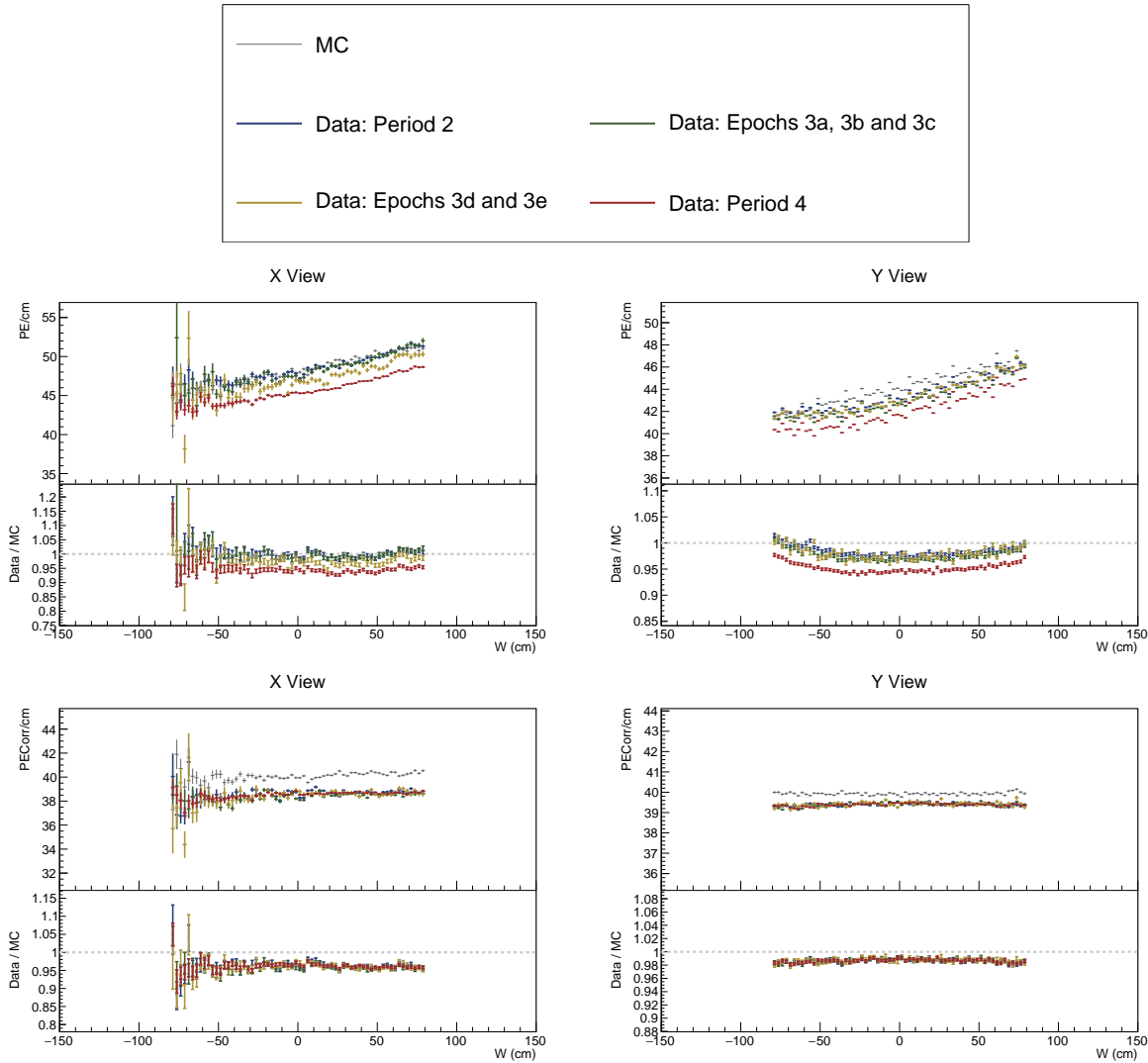


Figure 26: ...

- 532 [9] Alex Sousa. Test beam plenary update - fnal september 2018. NOVA Document 33012,
 533 September 2018. NOvA internal document. URL: <https://nova-docdb.fnal.gov/cgi-bin/sso>ShowDocument?docid=33012>.
- 535 [10] Karol Lang. Nova test beam: To mix, or not to mix, that is the question. NOVA Document
 536 34046-v2, November 2018. NOvA technical note. URL: <https://nova-docdb.fnal.gov/cgi-bin/sso>ShowDocument?docid=34046>.
- 538 [11] Alex Sousa. 2nd block filling status - nov. 18, 2019. NOVA Document 41961, November
 539 2019. NOvA internal document. URL: <https://nova-docdb.fnal.gov/cgi-bin/sso>ShowDocument?docid=41961>.
- 541 [12] Alex Sousa. Filling system and scintillator status. NOVA Document 34067, November
 542 2018. NOvA internal document. URL: <https://nova-docdb.fnal.gov/cgi-bin/sso>ShowDocument?docid=34067>.

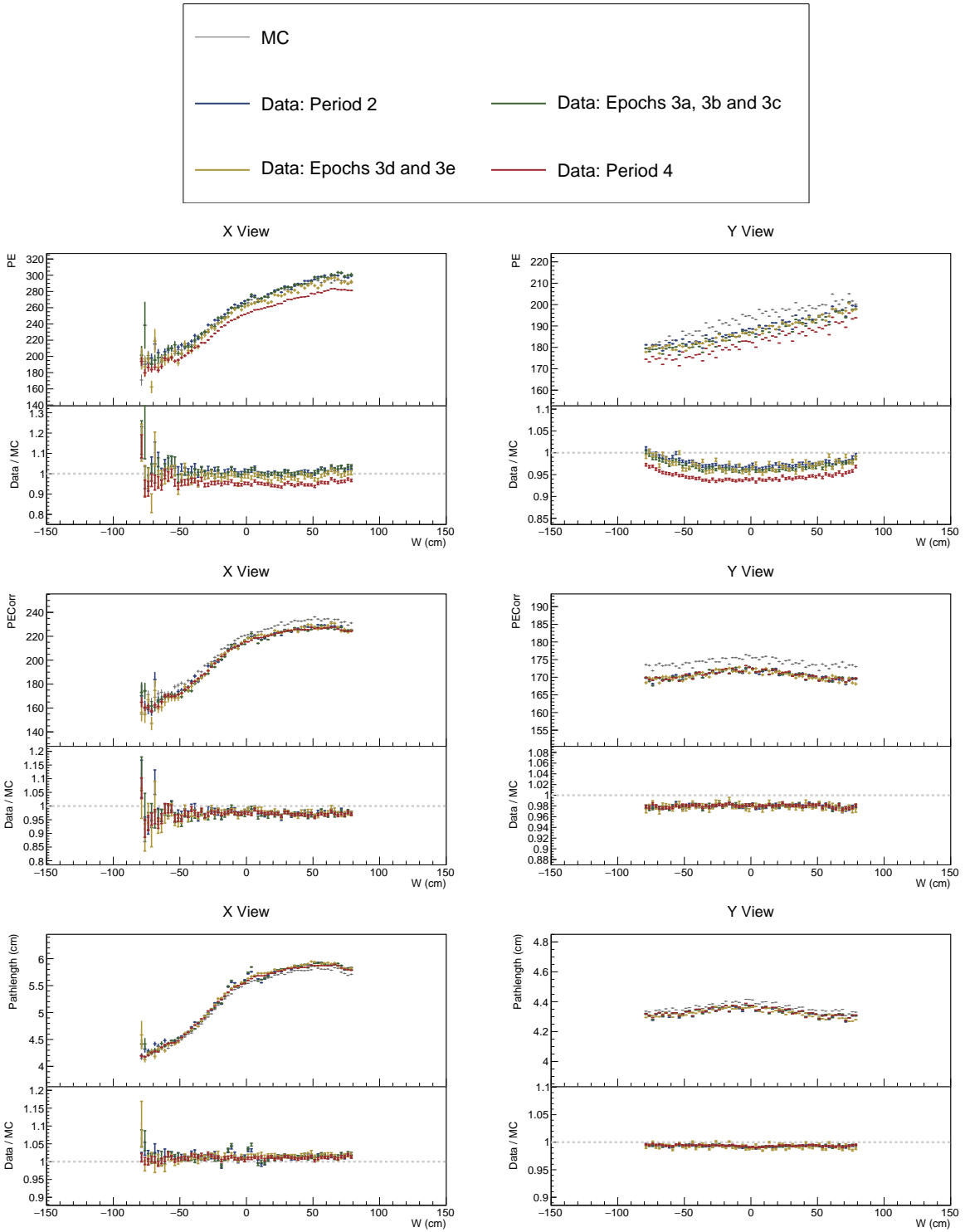


Figure 27: ...

[13] Beatriz Tapia Oregui Junting Huang, Will Flanagan. Test beam: Light yield of the liquid scintillator drained from the ndos detector. NOVA Document 38740, July 2019. NOVA internal document. URL: <https://nova-docdb.fnal.gov/cgi-bin/sso>ShowDocument?docid=38740>.

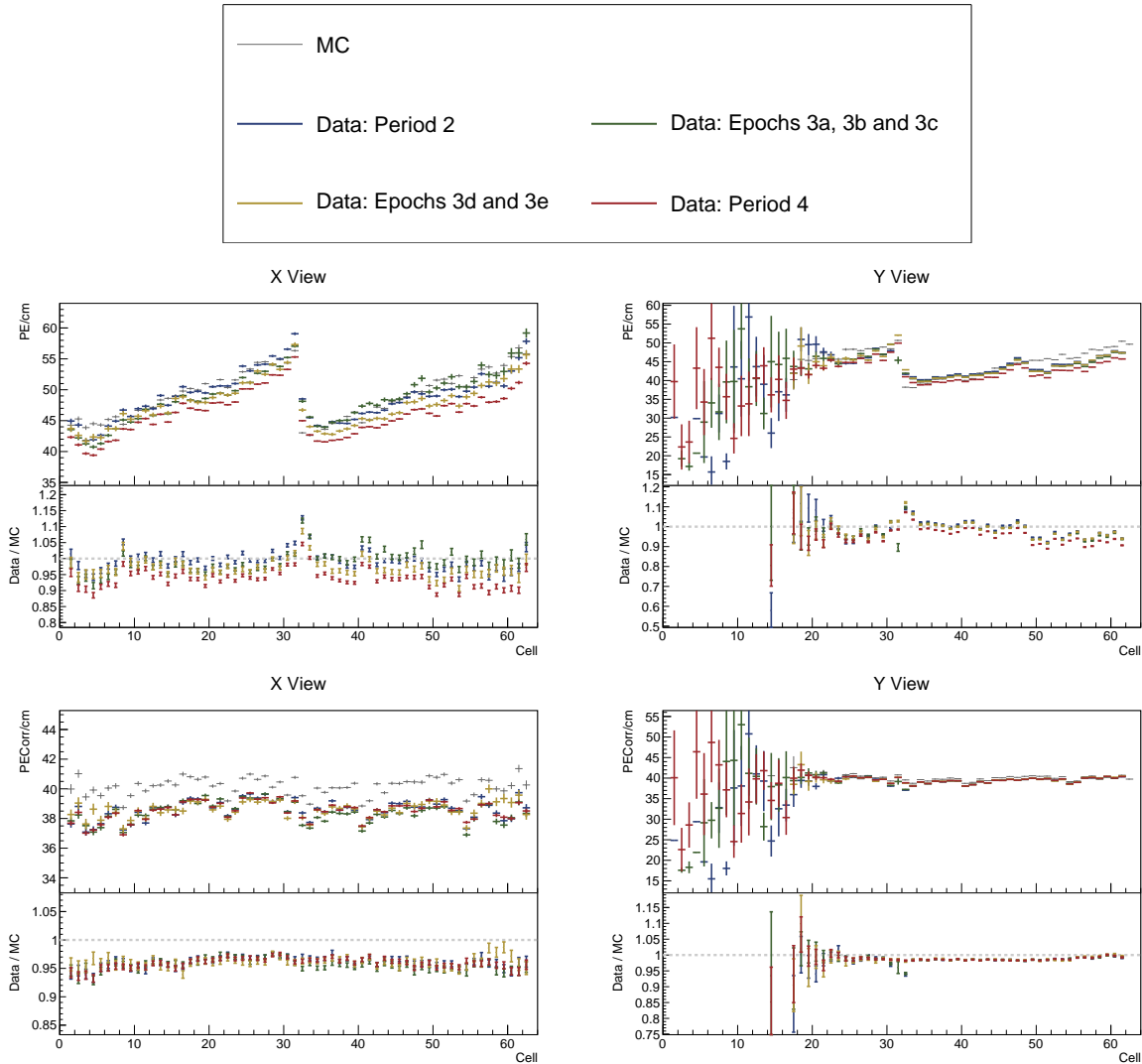


Figure 28: ...

- 548 [14] Dung Phan. Test beam: Tintometer measurement of texas a&m oil. NOVA Document
 549 39088, July 2019. NOvA internal document. URL: <https://nova-docdb.fnal.gov/cgi-bin/sso>ShowDocument?docid=39088>.
- 551 [15] Teresa Megan Lackey. *Proton Scattering in NOvA Test Beam*. PhD thesis, Indiana U., 7
 552 2022.
- 553 [16] Yagmur Torun David Northacker, Alex Sousa. Test beam - overfilling horizontal planes.
 554 NOVA Document 49439, March 2021. NOvA internal document. URL: <https://nova-docdb.fnal.gov/cgi-bin/sso>ShowDocument?docid=49439>.
- 556 [17] Madbh A. A. Campbell Tyler Alion et al. Calibration technotes. NOVA Document
 557 13579, September 2017. NOvA technical note. URL: <https://nova-docdb.fnal.gov/cgi-bin/sso>ShowDocument?docid=13579>.

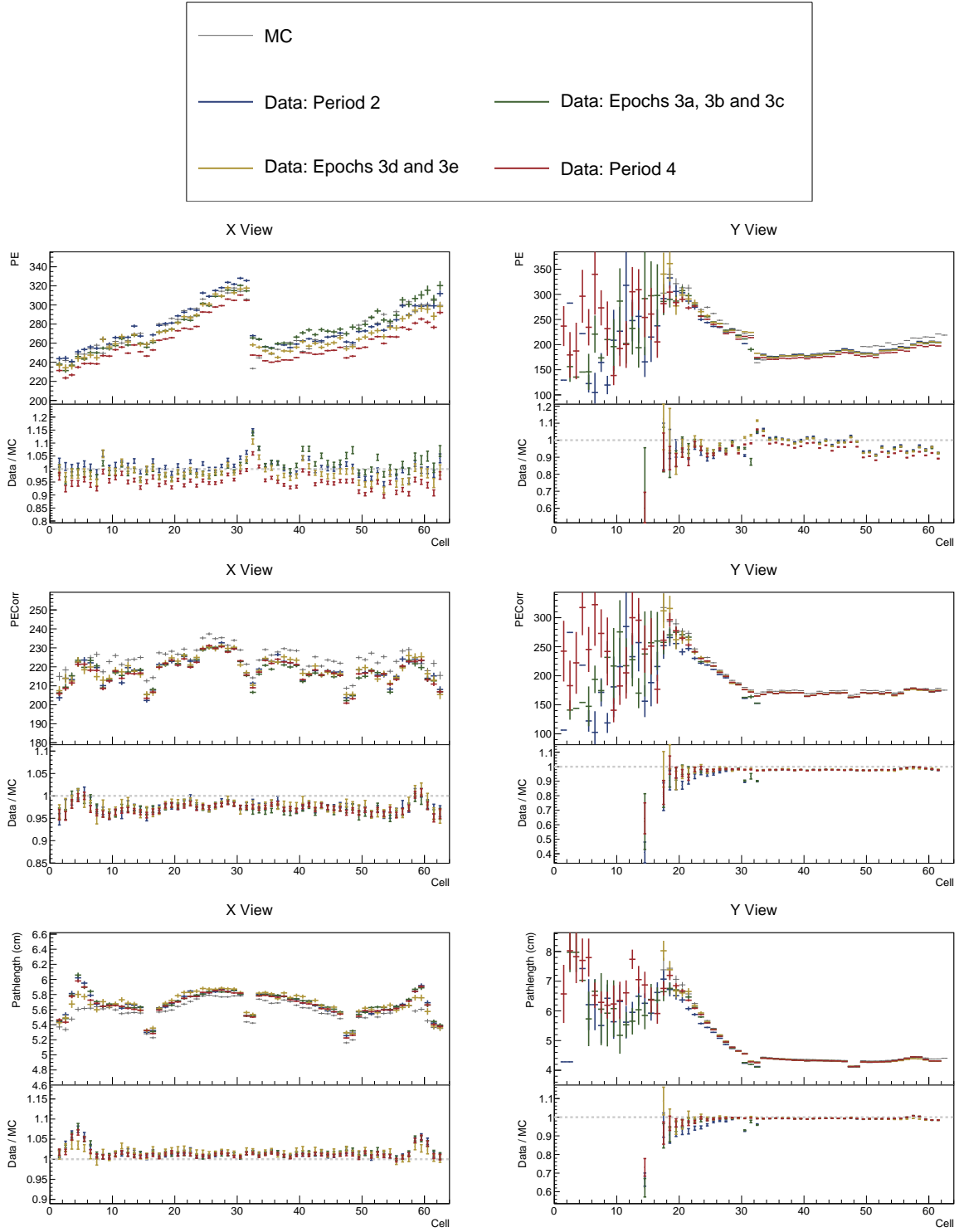


Figure 29: ...

559 [18] Christopher J Backhouse. Cell-by-cell attenuation calibration of the nova detectors.
 560 NOVA Document 7410, December 2014. NOvA technical note. URL: <https://nova-docdb.fnal.gov/cgi-bin/sso>ShowDocument?docid=7410>.

562 [19] Evan David Niner. *Observation of Electron Neutrino Appearance in the NuMI Beam with*

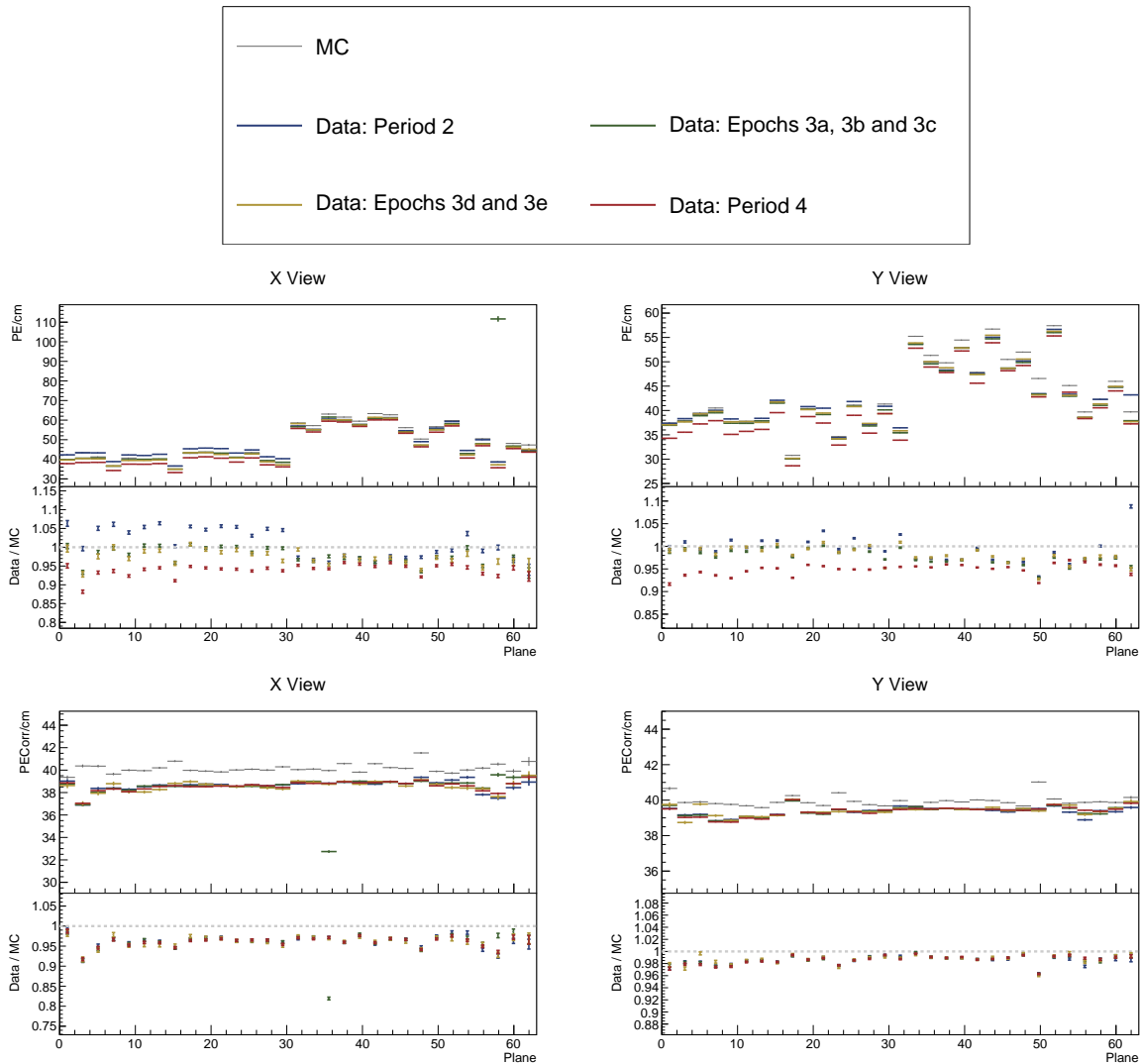


Figure 30: ...

- 563 *the NOvA Experiment*. PhD thesis, Indiana U., 2015. doi:10.2172/1221353.
- 564 [20] Christopher J Backhouse. Timing bias introduced by incorrect interpretation of the
565 nanoslice. NOVA Document 13518, June 2015. NOvA technical note. URL: <https://nova-docdb.fnal.gov/cgi-bin/sso>ShowDocument?docid=13518>.
- 566 [21] Luke Vinton. Calorimetric energy scale calibration of the nova detectors. NOVA Docu-
567 ment 13579, July 2015. NOvA technical note, FA_Calorimetric_energy_scale.pdf. URL:
568 <https://nova-docdb.fnal.gov/cgi-bin/sso>ShowDocument?docid=13579>.
- 569 [22] Keith Matera. Keith's swell guide: The calibration meta. NOVA Document 13579, Jan-
570 uary 2017. NOvA technical note, Calibration_Meta_READFIRST.pdf. URL: <https://nova-docdb.fnal.gov/cgi-bin/sso>ShowDocument?docid=13579>.
- 571 [23] Prabhjot Singh Christopher Backhouse, Alexender Radovic. The attenuation and thresh-
572 old calibration of the nova detectors. NOVA Document 13579, May 2016. NOvA techni-
- 573

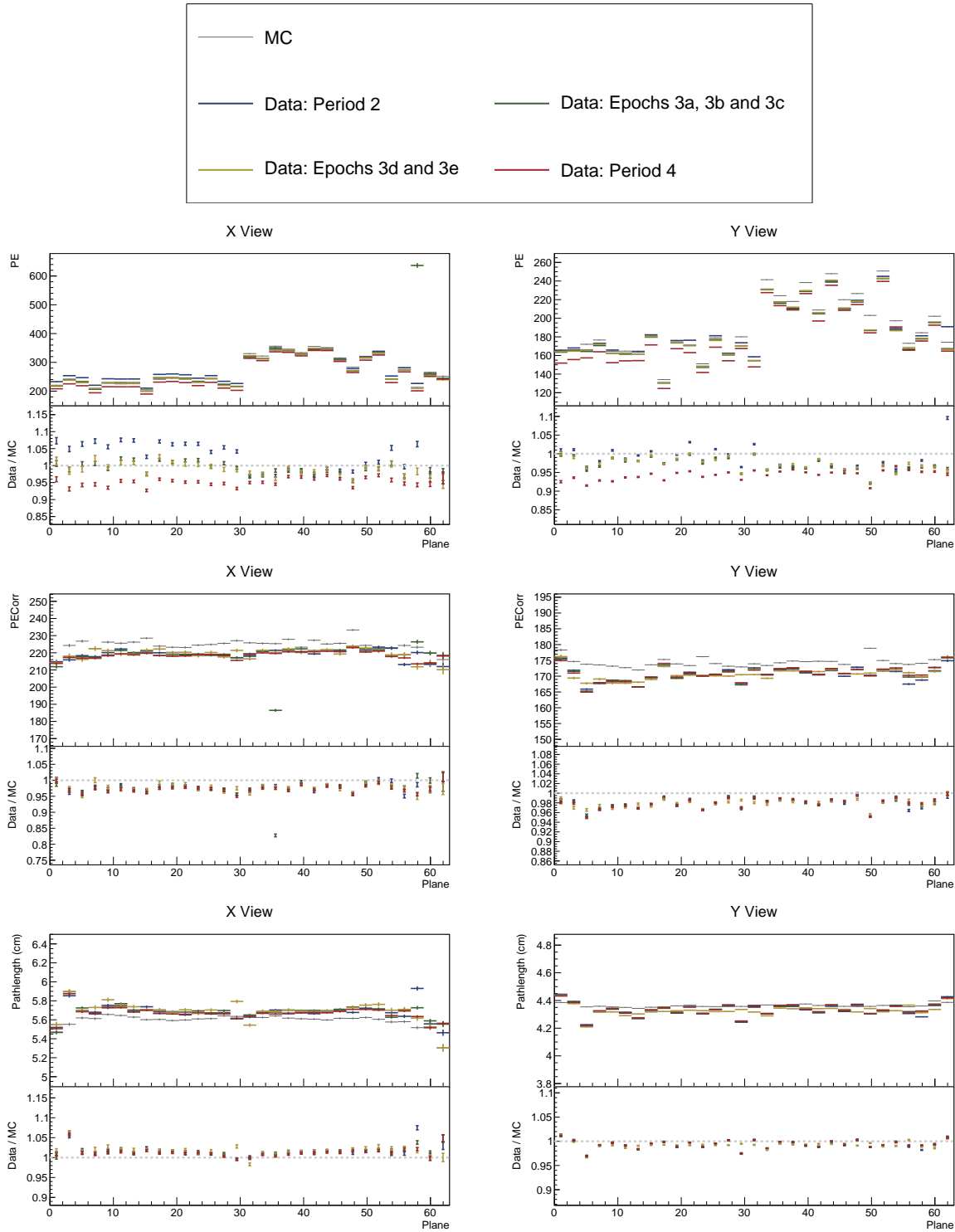


Figure 31: ...

575 cal note, SA_Attenuation_and_Threshold.pdf. URL: <https://nova-docdb.fnal.gov/cgi-bin/sso>ShowDocument?docid=13579>.

576 [24] Ryan J Nichol. Fibre brightness from cosmic muon data. NOVA Document 34909, De-
577 cember 2018. NOvA technical note. URL: <https://nova-docdb.fnal.gov/cgi-bin/>

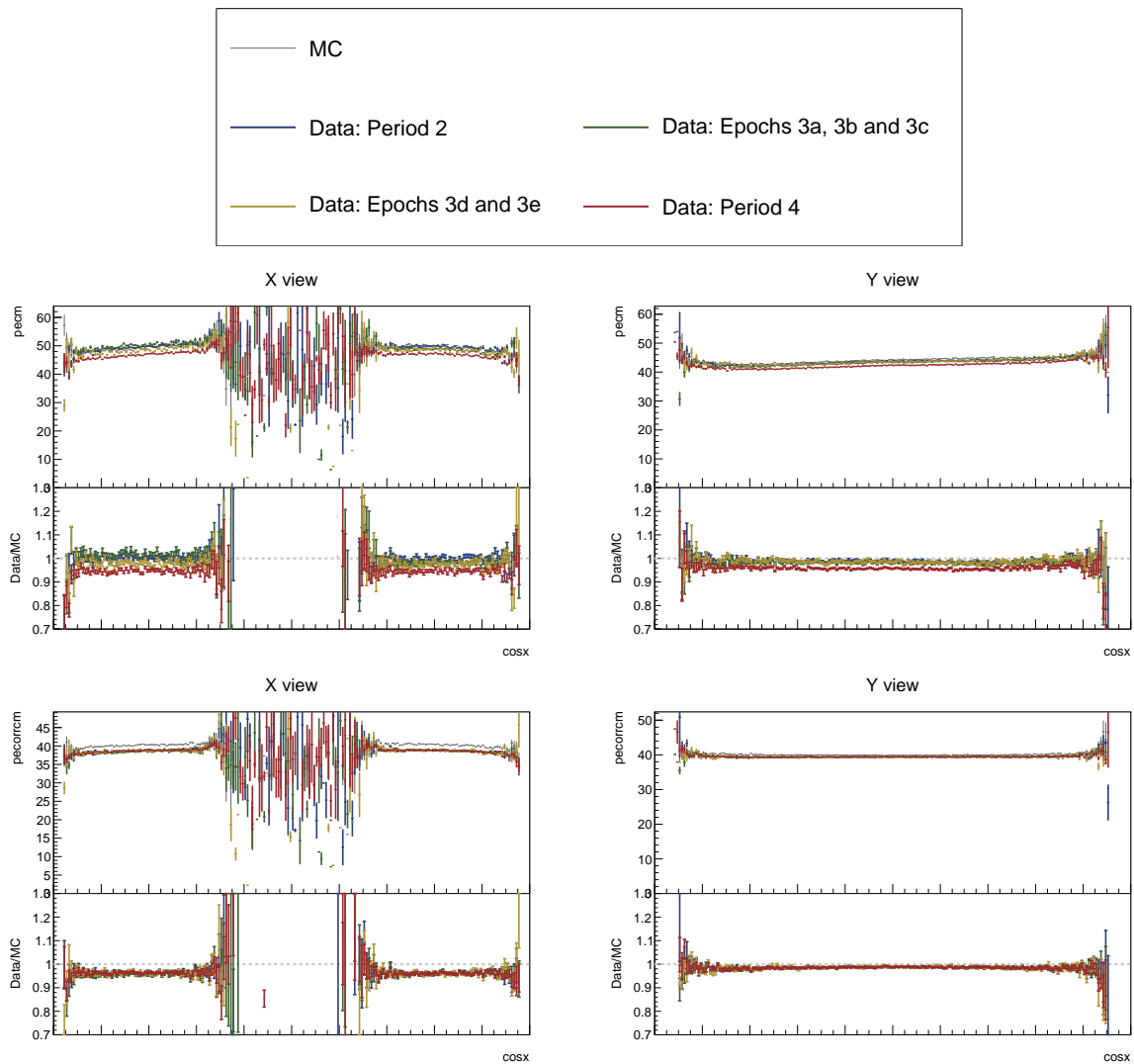


Figure 32: ...

579

sso/ShowDocument?docid=34909.

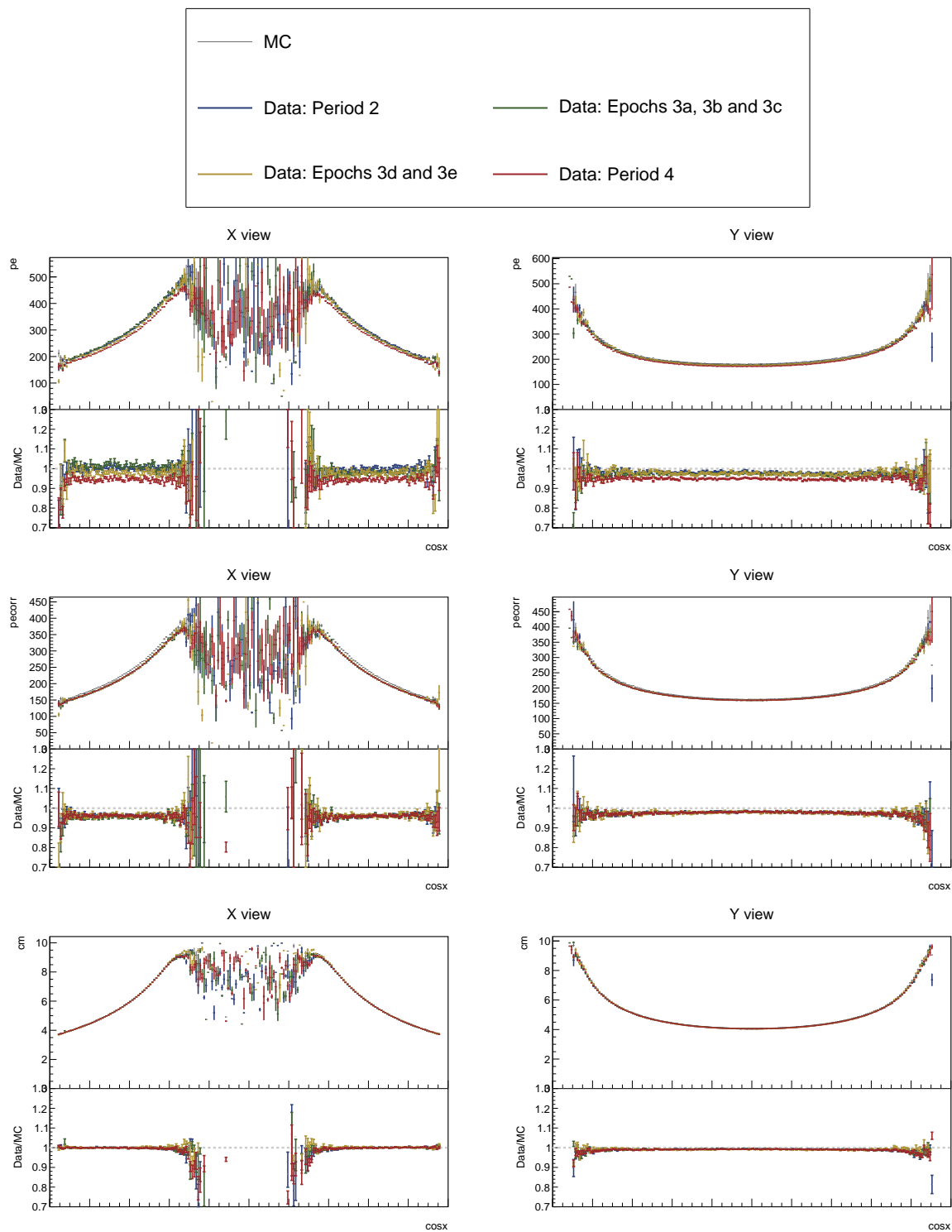


Figure 33: ...

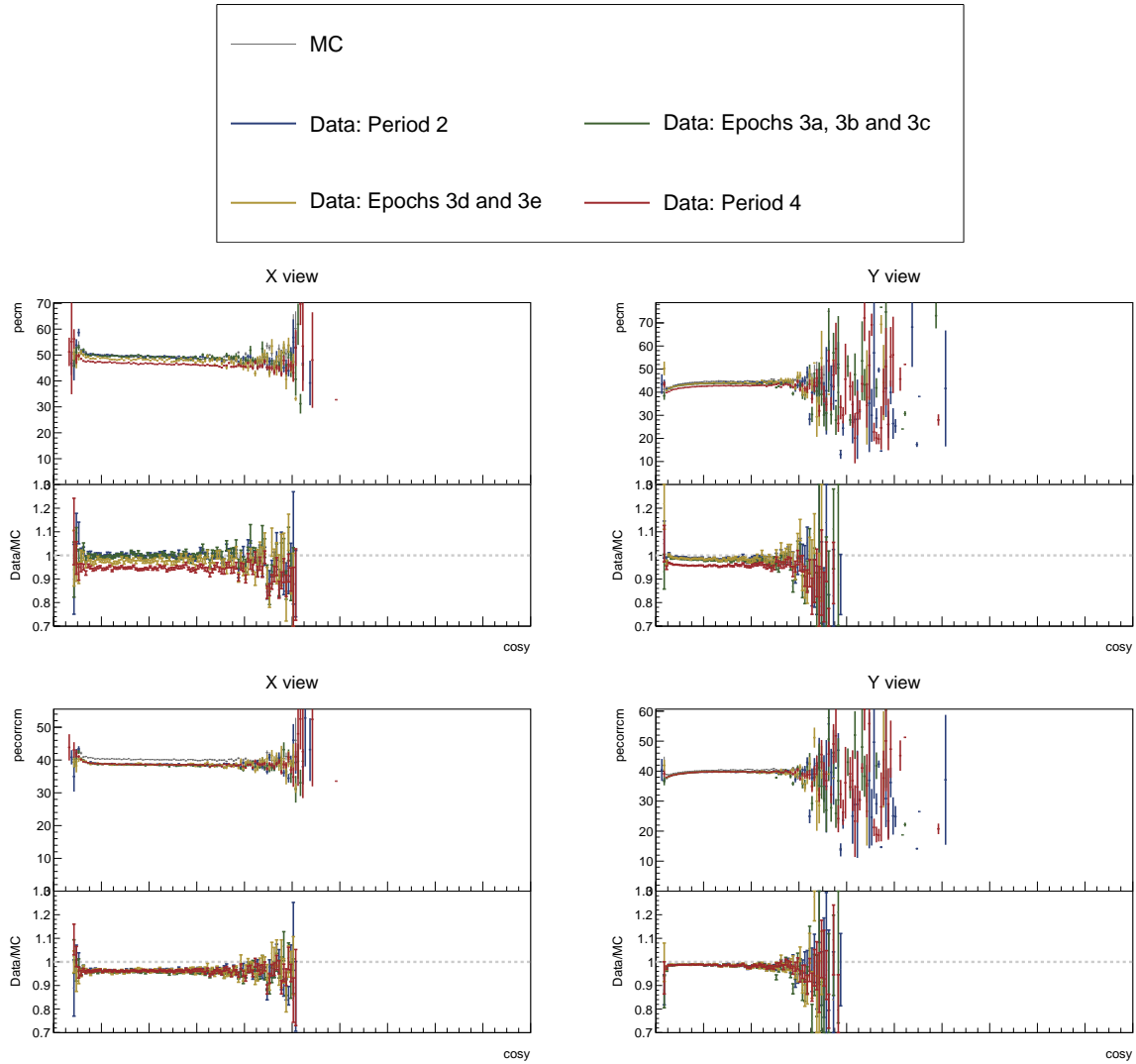


Figure 34: ...

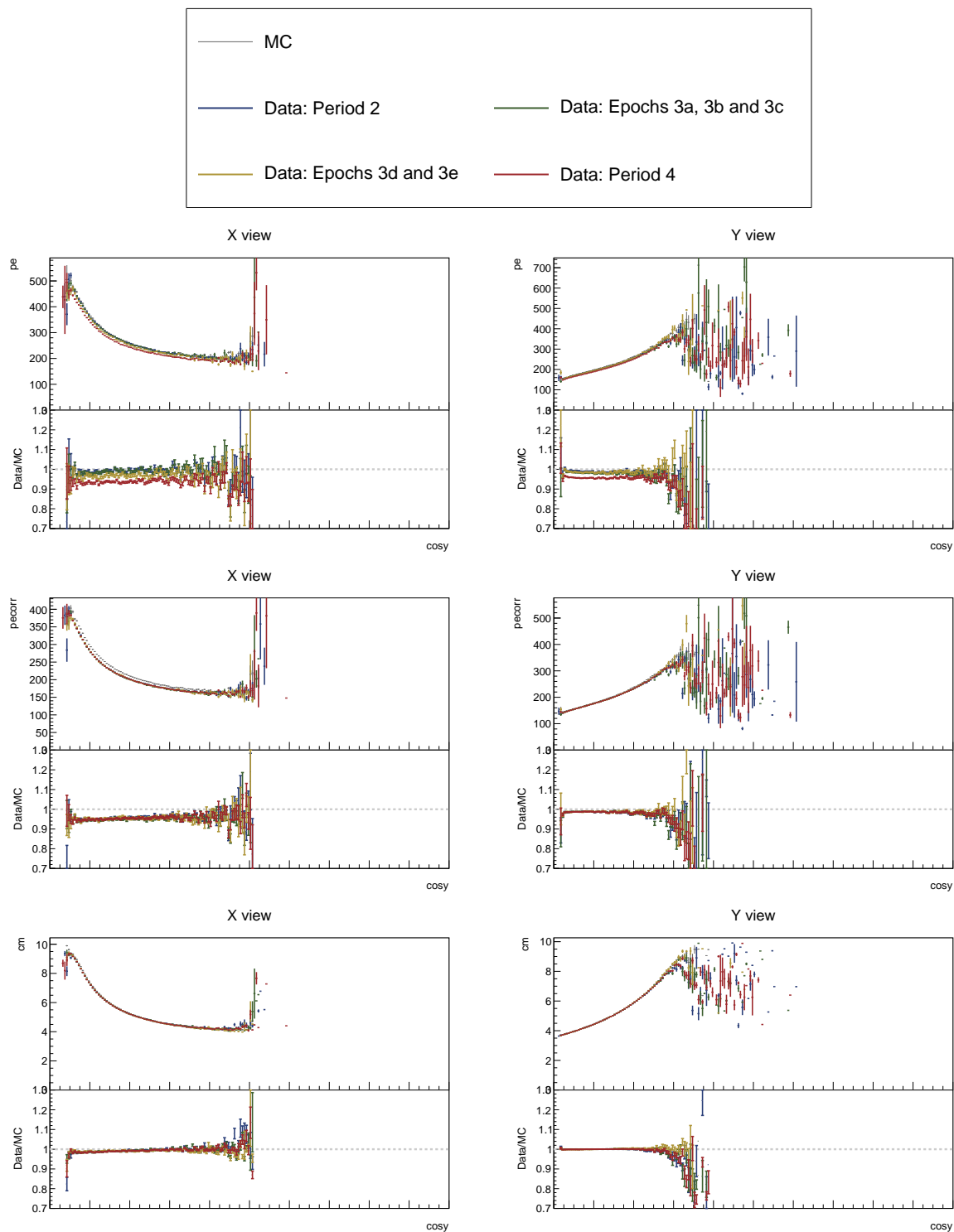


Figure 35: ...

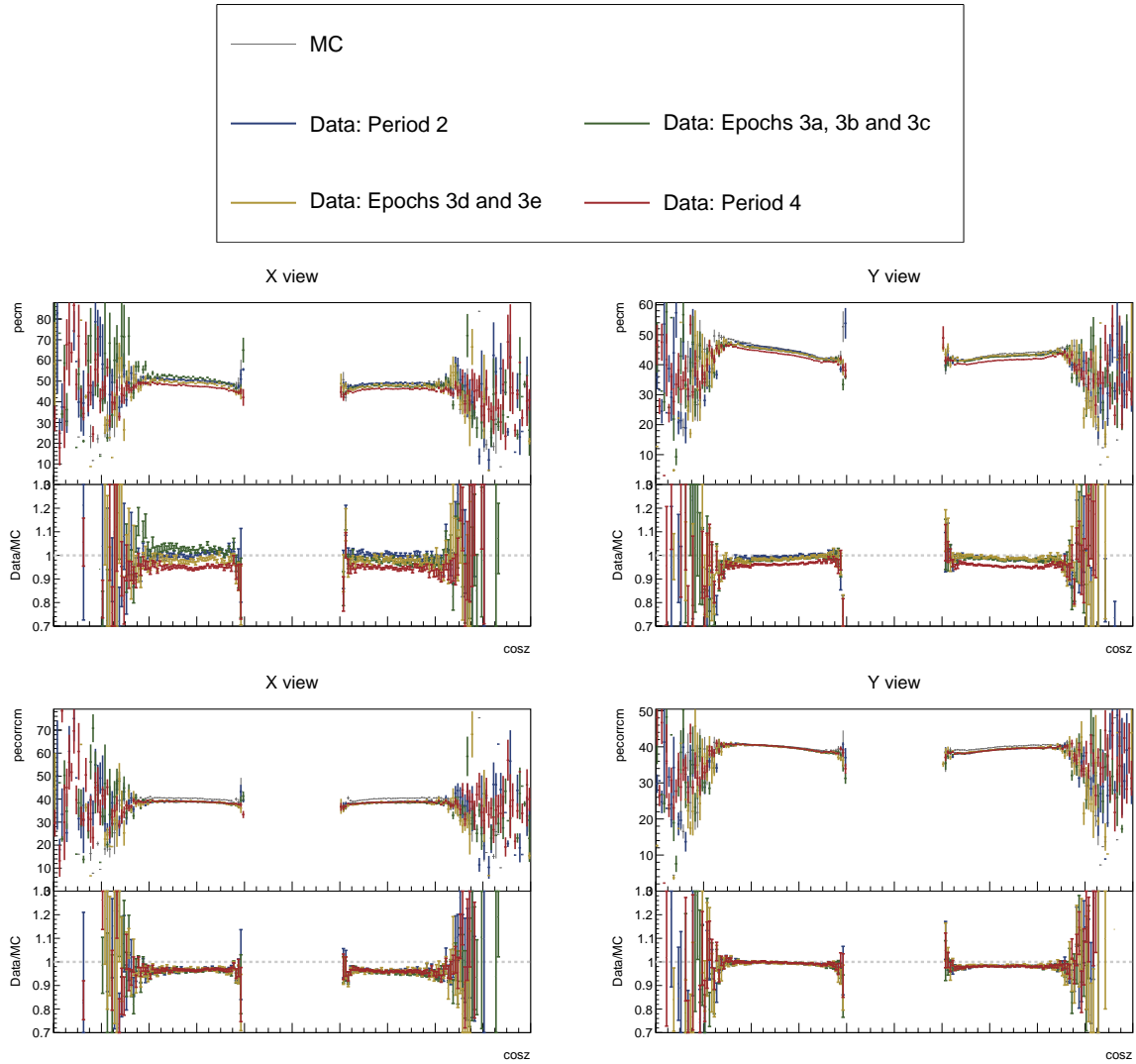


Figure 36: ...

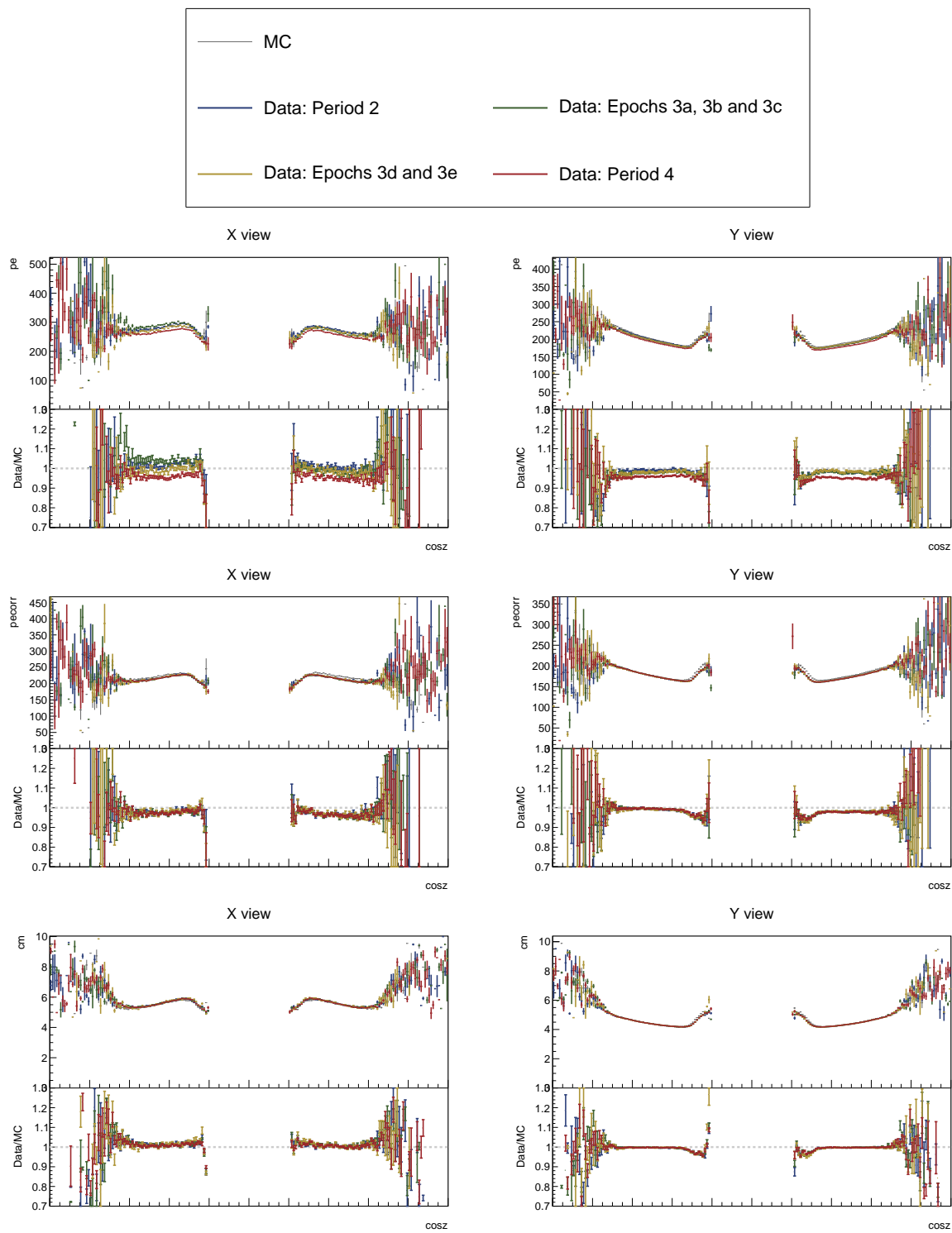


Figure 37: ...

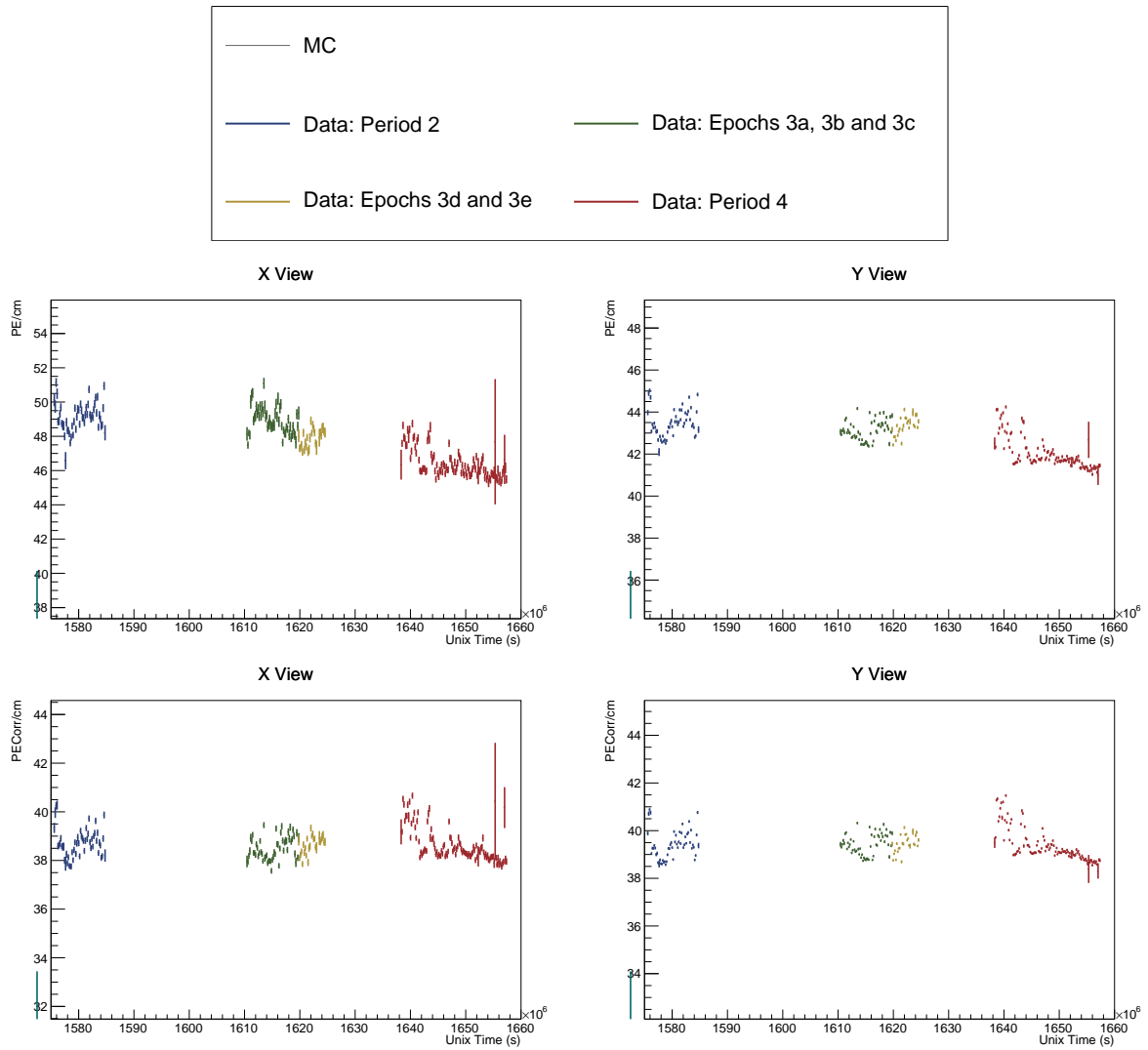


Figure 38: ...

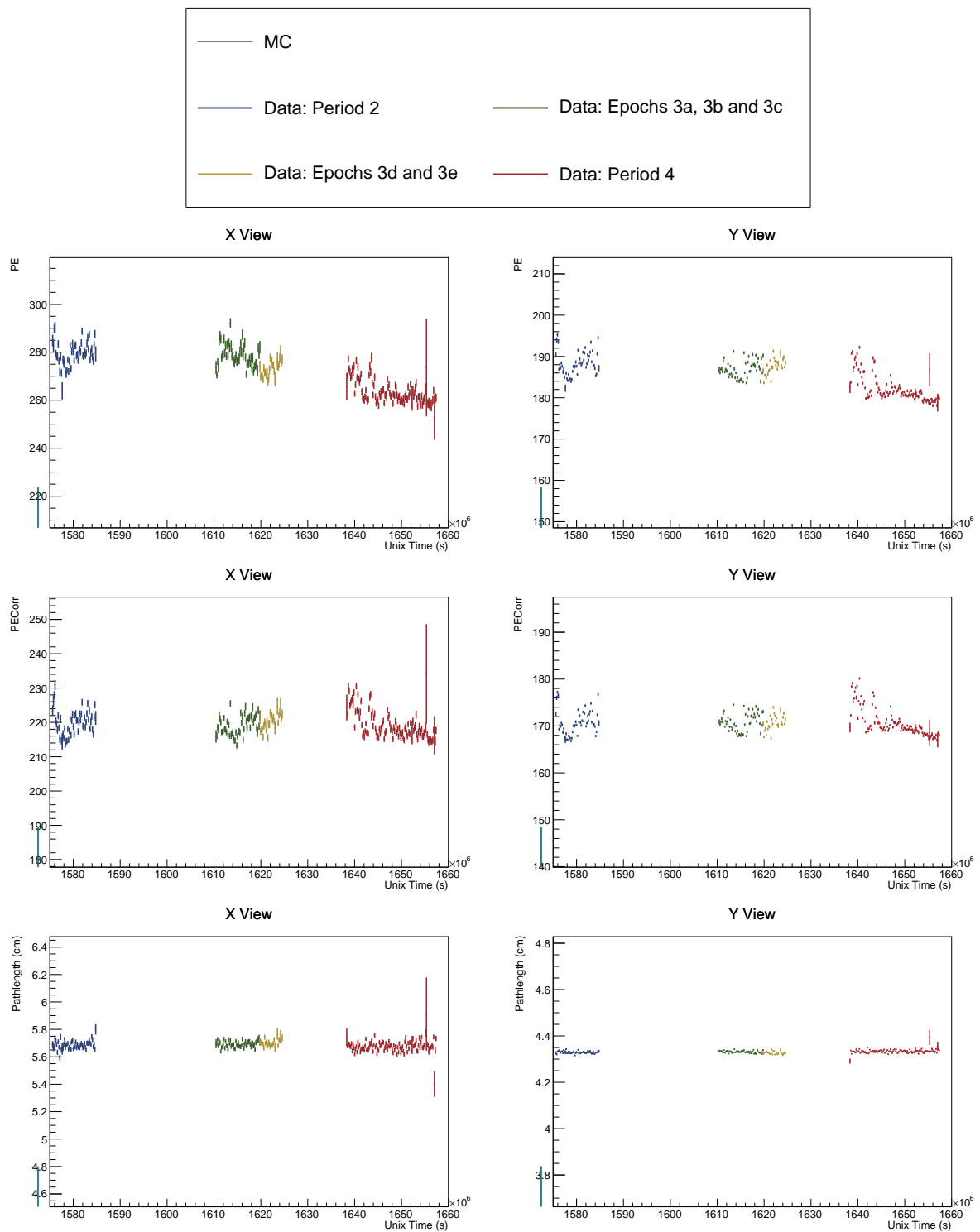


Figure 39: ...